

1  
2  
3  
4  
5  
6  
7  
8  
9  
10  
11  
12  
13  
14  
15  
16  
17  
18  
19  
20

# **Lunar Irregular Mare Patches (IMPs): Classification, Characteristics, Geologic Settings, Updated Catalog, Origin and Outstanding Questions**

**Le Qiao<sup>1,2</sup>, James W. Head<sup>3</sup>, Zongcheng Ling<sup>1</sup>, and Lionel Wilson<sup>4</sup>**

<sup>1</sup>Shandong Key Laboratory of Optical Astronomy and Solar-Terrestrial Environment, School of Space Science and Physics, Institute of Space Sciences, Shandong University, Weihai, Shandong, 264209, China.

<sup>2</sup>Key Laboratory of Lunar and Deep Space Exploration, Chinese Academy of Sciences, Beijing 100101, China

<sup>3</sup>Department of Earth, Environmental and Planetary Sciences, Brown University, Providence, RI 02912, USA.

<sup>4</sup>Lancaster Environment Centre, Lancaster University, Lancaster LA1 4YQ, UK.

Corresponding authors: Le Qiao (leqiao.geo@gmail.com), Zongcheng Ling (zcling@sdu.edu.cn)

## **Key Points:**

- We present an updated catalog of 91 lunar Irregular Mare Patches (IMPs) and survey the geologic settings and characteristics of each IMP
- Two classification schemes for the entire IMP population are proposed on the basis of their geologic settings and characteristics
- The characteristics of lunar IMPs are consistent with the waning-stage magmatic foam extrusion origin model in different environments

## 21 **Abstract**

22 One of the most mysterious lunar features discovered during the Apollo era was Ina, a  $\sim 2 \times 3$  km  
23 depression composed of bleb-like mounds surrounded by hummocky and blocky terrains.  
24 Subsequent studies identified dozens of similar features in lunar maria, describing them as  
25 Irregular Mare Patches (IMPs). Due to the unusual and complex characteristics of IMPs, their  
26 specific formation mechanism is debated. To improve our understanding of the nature and origin  
27 of IMPs, we undertook an updated search and geological characterization of all IMPs and  
28 established a classification approach encompassing the full spectrum of IMPs. We present an  
29 updated catalog of 91 IMPs and survey the detailed characteristics of each IMP. We find that the  
30 majority of IMPs occur in maria emplaced over three billion years ago, contemporaneous with  
31 the peak period of global lunar volcanism. We utilized geologic context information and  
32 characteristics to establish two classification schemes for lunar IMPs: 1) Geologic context: IMPs  
33 are categorized into a) small shield volcano summit pit floor and flank, b) linear/sinuuous rille  
34 interior and adjacent exterior, and c) typical maria; 2) Characteristics: IMPs are classified into a)  
35 “mound + floor” and b) “pit only” types. We showed the rang of characteristics of lunar IMPs  
36 were consistent with the waning-stage magmatic foam formation and extrusion scenario in  
37 different environments. Our updated catalog and classification raise several outstanding  
38 questions concerning the nature and origin of lunar IMPs. Assessing these questions will  
39 improve our knowledge of lunar thermal and geologic evolution.

## 40 **Plain Language Summary**

41 Composed of fresh-looking bulbous-shaped mounds surrounded by a hummocky and blocky  
42 floor, the  $2 \times 3$  km Ina depression is one of the most enigmatic and poorly understood features  
43 discovered during early lunar exploration. Later studies identified dozens of similar features in  
44 the lunar maria and named them Irregular Mare Patches (IMPs). To achieve an improved  
45 knowledge of IMPs, we undertook an updated search, geologic analysis and classification study  
46 of all currently known IMPs, presenting a combined catalog of 91 IMPs. We find that the  
47 majority of lunar IMPs occur in mare units emplaced over three billion years ago, coinciding  
48 with the peak period of global lunar volcanism. We then classified the entire IMP population on  
49 the basis of their geologic settings and characteristics, and documented and classified the detailed  
50 surface texture of the floor terrains at each IMP site. This new and updated detailed  
51 characterization and classification of the entire IMP population provides important new  
52 information about their nature and origin. Association with volcanic vent areas and ancient  
53 volcanic structures and deposits suggests that late stage volcanic degassing processes during the  
54 period of mare volcanism  $>3$  Ga ago should be considered in more detail.

## 55 **1. Introduction**

56 One of the most unusual lunar surface features discovered and studied during the Apollo era  
57 was the Ina feature. It was first identified by Ewen A. Whitaker on Apollo 15 panoramic camera  
58 photography (Figure 1B), notable for its unique D-shaped appearance (Whitaker, 1972) and  
59 unusual interior structure. This feature had actually been imaged on a pre-Apollo Lunar Orbiter  
60 photograph (frame IV-102-H3), but unfortunately missed due to being partially obscured by film  
61 processing defects (bi-mat bubbles) (Figure 1A). Subsequent detailed photogeological studies by  
62 Farouk El-Baz and his colleagues (El-Baz, 1972, 1973; Evans & El-Baz, 1973; Strain & El-Baz,  
63 1980) informally designated Ina as “D-Caldera” and presented many observations concerning its

64 characteristics and possible mode of origin (Figures 1B-E). The name “Ina” appeared first in a  
 65 topophotomap published by NASA in 1974 (sheet 41C3S1(10)) and was then approved by the  
 66 International Astronomical Union in 1979, along with the nomenclature *Mons Agnes* for the  
 67 major mound at the eastern interior floor margin (Figure 1B).

68 Re-analyses of Apollo imaging data sets found that Ina-like features were not unique;  
 69 similar but much smaller depressions were identified having reflective, rubbly floors bounded by  
 70 irregular, highly reflective scarps in three locations: (1) on the floor of Hyginus crater (Schultz,  
 71 1976; 7.726°N, 6.350°E), (2) along the extension of a graben in SW Mare Tranquillitatis  
 72 (Schultz, 1976; 4.096°N, 21.218°E) and (3) along the western edge of Mare Serenitatis  
 73 (Masursky, 1978; a group of small depressions at 24.773°N, 8.045°E, Aratus D-1 to 3 in Table  
 74 1). Newly acquired sub-meter-scale Lunar Reconnaissance Orbiter Narrow Angle Cameras  
 75 (LROC NAC) images enable the identification of dozens of new features on mare surfaces with  
 76 similar morphologies. Stooke (2012) initiated this campaign and found 23 additional Ina-like  
 77 features (termed “meniscus hollows”) in several mare locations: west edge of Mare Serenitatis (n  
 78 = 3; near to those found in Masursky, 1978), NW Mare Tranquillitatis (n = 7), West Mare  
 79 Fecunditatis (n = 6), northern margin of Mare Insularum (n = 4), SW corner of Mare Imbrium (n  
 80 = 1), the vicinity of a rille in Oceanus Procellarum (n = 1) and eastern margin of Sinus Aestuum  
 81 (n = 1). Braden et al. (2014) pursued this work and expanded the inventory to 70 features in mare  
 82 regions in the central nearside of the Moon and described them as irregular mare patches (IMPs).  
 83 Moreover, several ensuing lunar morphological investigations found additional sporadic IMP  
 84 occurrences (e.g., Zhang et al., 2018).

## 85 1.1 Theories for the Origin of IMPs

86 A half-century after the discovery of Ina, the most notable IMP feature, during the Apollo  
 87 era, the mechanism(s) of origin, mode of emplacement and age (either ancient or geologically  
 88 very recent) of IMPs are still being debated (e.g., El-Baz, 1973; Strain & El-Baz, 1980; Schultz  
 89 et al., 2006; Garry et al., 2012; Braden et al., 2014; Qiao et al., 2017, 2018a, 2019a). A summary  
 90 of these previously-proposed theories for the origin of lunar IMPs and their associated deposits is  
 91 outlined in Table 1, and more comprehensive details can be found in the references indicated and  
 92 in Qiao et al. (2019a). These prior investigations have documented substantial observations of  
 93 lunar IMPs, including geologic settings, topography, morphology, morphometry, optical  
 94 reflectance and maturity, composition from visible, near-infrared and thermal-infrared  
 95 spectroscopy, thermophysical properties, surface physical properties, photometry and superposed  
 96 impact crater populations and their constraints on previously proposed mechanisms of origin  
 97 (e.g., Strain & El-Baz, 1980; Garry et al., 2012; Garry et al. 2013; Braden et al., 2014; Bennett et  
 98 al. 2015; Donaldson Hanna et al., 2016; Grice et al., 2016; Neish et al., 2017; Elder et al., 2017;  
 99 Qiao et al., 2017, 2018a, 2019a; Glaspie et al., 2019; and references therein).

100 These substantial observational results and many different and competing theories (Table 1)  
 101 have raised a line of key questions concerning the nature and origin of lunar IMPs: (1) What is  
 102 the origin of the various floor terrain textures? (2) What is the thickness and variability of the  
 103 surface regolith layer? (3) What is the reason for the anomalous surface immaturity? (4) How are  
 104 the relatively steep walls and slopes maintained? (5) How do the mineralogy and composition  
 105 compare with those of surrounding units? (6) What are their ages and the causes, including (6a)  
 106 what is the emplacement age of the deposits of lunar IMPs? (6b) what is the age relationship

107 between mounds and floor units? (6c) how do the ages derived from impact crater size-frequency  
108 distributions (CSFD) compare with those of surrounding units?

109 Among the major difficulties in resolving the origin of IMPs are their highly variable  
110 characteristics and geological settings, both between different IMP occurrences and among  
111 different parts of some specific IMP features. Apollo-era analyses had already noted the major  
112 morphological variations of Ina floor terrains, including bright rough-textured units, polygonal  
113 hummocks and dark hilly terrains (Strain & El-Baz, 1980). Updated LROC NAC-based  
114 morphological investigations documented substantial new textural properties of the floor of Ina,  
115 e.g., pitted, ridged, polygonal and vermicular textures (Qiao et al., 2019a). In addition, apart  
116 from several major IMP occurrences (e.g., Ina, Sosigenes, Cauchy-5 and Hyginus), the detailed  
117 geological characteristics of the majority of lunar IMPs, including geologic setting,  
118 geomorphology, morphometry and surface texture, were not well documented. Earlier  
119 inspections based on Apollo photographs had revealed the similarity in morphology between Ina  
120 and other IMP features, while also noting the apparent differences. For example, the IMPs  
121 identified in three other locations are more than one order of magnitude smaller than the Ina  
122 feature (maximum length: 40–170 m vs. 2.9 km) and lack the raised mounds observed at Ina  
123 (Schultz, 1976, 1991). Recent preliminary analyses using LROC NAC images also noted the  
124 wide range of dimensions, structures and characteristics of the documented IMPs (e.g., Braden et  
125 al., 2014; Qiao et al., 2019b). In order to develop an improved understanding of the formation  
126 mechanism of the entire cataloged IMP population, it is necessary to conduct a thorough  
127 geological characterization of all the IMP occurrences and to establish classification schemes  
128 that take into account the full spectrum of characteristics of lunar IMPs.

129 In this contribution, we first present an updated, comprehensive catalogue of IMP  
130 occurrences on the basis of their identification from multiple prior studies. In order to understand  
131 the cataloged IMP population as a whole, we analyze the detailed geological characteristics of  
132 each IMP feature, including geologic setting, surface model age of the background mare unit,  
133 structure, geomorphology and surface texture. We then develop two IMP classification schemes  
134 that illustrate the spectrum of the geologic settings and characteristics of lunar IMPs and their  
135 variations. We also investigate the applicability of the waning-stage magmatic foam formation  
136 and extrusion scenario to the origin mechanism of our catalogued IMPs of various categories.  
137 We outline several outstanding questions raised by our characterization and classification  
138 schemes that need to be explained to understand the origin of IMPs and the constraints they place  
139 on the thermal and geologic evolution of the Moon.

## 140 **2. Data and Methods**

141 We first present an updated catalog of lunar IMPs by compiling multiple previous IMP  
142 identification studies, from Apollo-era investigations (Whitaker, 1972; Schultz, 1976) to recent  
143 LROC NAC image-based surveys (e.g., Stooke, 2012; Braden et al., 2014). We then analyze the  
144 geologic setting of each IMP occurrence, including the morphology, topography and tectonic  
145 setting, using the latest moderate-resolution images from the LROC Wide-Angle Camera (WAC,  
146 100 m/pixel, Robinson et al., 2010) and Kaguya Terrain Cameras (TC, 10 m/pixel, Haruyama et  
147 al., 2008), and altimetric data from the Kaguya TC stereogrammetry digital terrain model (DTM)  
148 (10 m pixel size and ~3–4 m altimetric accuracy; Haruyama et al., 2012; Barker et al., 2014) and  
149 Kaguya TC + LRO-LOLA (Lunar Orbiter Laser Altimeter) merged topography (SLDEM2015;  
150 512 pixels/degree spatial sampling and ~3–4 m vertical altimetric accuracy; Barker et al., 2016).

151 We also examine the detailed morphology, morphometry and surface texture of each IMP feature  
152 using high-resolution LROC NAC images (up to 0.47 m/pixel, Robinson et al., 2010). Each  
153 individual LROC NAC frame has been pre-processed from the raw NAC EDR (experiment data  
154 record) image through photometric correction and map-projection using the USGS's Integrated  
155 Software for Imagers and Spectrometers (ISIS3; e.g., Anderson et al. 2004) according to the  
156 terms of the LROC EDR Data Products Software Interface Specification (Bowman-Cisneros,  
157 2010). When high-resolution LROC NAC DTM topography (2–5 m/pixel and better than 2 m  
158 relative horizontal and vertical precision, Henriksen et al. 2017) is available (for 28 IMPs), the  
159 detailed topographic characteristics of these IMPs are also analyzed.

### 160 **3. An Updated IMP Catalogue of 91 IMPs**

161 We synthesize IMP occurrences from multiple sources beginning with the Apollo era  
162 investigations, namely, earlier identifications by Whitaker (1972), Schultz (1976) and Masursky  
163 (1978), the LROC NAC-based Stooke catalogue (Stooke, 2012), the Braden (2013) and Braden  
164 et al. (2014) catalog (Braden, 2013; Braden et al., 2014), two identifications by the recent Zhang  
165 et al. work (2018) and several identifications by amateur scientists from THE MOON wiki site  
166 ([https://the-moon.us/wiki/Irregular\\_Mare\\_Patches\\_\(IMPs\)](https://the-moon.us/wiki/Irregular_Mare_Patches_(IMPs))) (Tables 2 and 3). Each reported IMP  
167 occurrence has been visually checked and confirmed on meter-scale LROC NAC images. In  
168 total, our updated catalog includes 91 IMPs (Figure 2 and Table 3). IMPs identified in addition to  
169 the population in the Braden et al. (2014) catalog are listed in Table 2 and illustrative NAC  
170 images are shown in Figure 3. Several previously reported IMP identifications are not catalogued  
171 here because of their poor resolution on NAC images (either due to their small size or the  
172 relatively coarser available NAC image spatial resolution). Of the 21 additional IMPs, 11 are  
173 smaller than 100 m (note that Braden et al. (2014) only listed IMP occurrences larger than 100  
174 m).

### 175 **4. General characterization of all IMPs**

176 Prior documentation had shown the widespread distribution of IMPs across many nearside  
177 maria (Braden et al., 2014) and our updated catalog further expands the known IMP occurrences  
178 into two additional nearside basin-filling maria: Mare Serenitatis (Aratus D IMPs) and Mare  
179 Imbrium (Brayley D IMP) (Figure 2). The most concentrated region of IMPs is in western Mare  
180 Tranquillitatis (35 IMPs); though not entirely within the Procellarum KREEP Terrane (PKT;  
181 Jolliff et al., 2000), this region is characterized by a regional enrichment of thorium abundance  
182 (~3–5 ppm; Lunar Prospector Gamma-Ray Spectrometer 0.5° thorium data deconvolved by  
183 Lawrence et al., 2003). Another IMP-concentrated region (18 IMPs) near Gruithuisen E and M  
184 craters (within PKT) also shows regionally elevated thorium content (~8.5–9.5 ppm). The reason  
185 for the presence of small clusters of IMPs in particular mare locations is uncertain from the  
186 available observations and analyses. The west Mare Tranquillitatis region displays many NNE-  
187 SSW-trending graben and wrinkle ridges, which appear to be concentric to the Tranquillitatis  
188 basin center (Yue et al., 2015). Six small shield volcanoes are also observed in this region (Head  
189 & Gifford, 1980). The Gruithuisen E and M region contains a group of small mare basaltic  
190 deposits scattered on the feldspathic ejecta from the Iridum crater. This area is adjacent to the  
191 Gruithuisen silicic domes (6–120 km; Ivanov et al., 2016) and some sinuous rilles (14–75 km),  
192 including Rima Sharp, the longest sinuous rille on the Moon (Hurwitz et al., 2013). It is  
193 unknown whether the concentration of lunar IMPs in these regions is related to these observed  
194 structures. A synthetical analysis of the regional geological context and tectonic setting,

195 topography, morphology, composition (iron, titanium, thorium, etc.) and the association between  
 196 various geologic features (mare domes, sinuous rilles, wrinkle ridges, graben, etc.) will  
 197 potentially shed light on this issue.

198 The identified IMPs are observed to vary in their longest dimension, spanning over one  
 199 order of magnitude (ranging from <100 m to 5 km; Table 3). Smaller IMPs are more common,  
 200 with 78% (n = 71) of IMPs less than 400 m and 51% (n = 47) of IMPs less than 200 m (Figure  
 201 4A).

202 The host mare units of 55 IMPs have been dated through the superposed impact crater size-  
 203 frequency distribution (CSFD) method (see sources in Figure 5 caption) and 14 IMPs are located  
 204 in undated mare units, while adjacent to other dated mare units (Table 3). In total, 69 IMPs are  
 205 located in or near 17 CSFD-dated mare units (Figures 4B and 5). Most of the 69 IMPs (n = 60,  
 206 87%) are observed to be hosted in mare units that were emplaced between 3.0 and 3.73 Ga ago,  
 207 contemporaneous with the peak of global lunar volcanism, between ~3.3 and 3.8 Ga ago (313  
 208 among the 482 (~65%) dated global mare units; Figure 5). Only nine IMPs are located in two  
 209 mare units emplaced later in the west nearside maria within the PKT terrain: (1) eight IMPs  
 210 occurs in a very local region in SW Mare Imbrium and NW Mare Insularum (the Bessarion V  
 211 IMPs and the Brayley D IMP), which are all located in or near the P43 mare unit (2.12 Ga;  
 212 Hiesinger et al., 2011a), and (2) another IMP (the Aristarchus North IMP; see more detailed  
 213 characterization of this IMP in section 5 below) occurs in the P60 mare unit in Oceanus  
 214 Procellarum (1.2 Ga; Hiesinger et al., 2011a), adjacent to Aristarchus crater ejecta.

## 215 5. Geologic Settings and the Classification Scheme

216 We investigate the detailed geologic settings of each IMP occurrence using the latest image  
 217 and altimetric data sets, including morphology, morphometry, topography and geologic/tectonic  
 218 setting, and propose a classification scheme of the geologic settings of the entire documented  
 219 IMP population as follows (Figure 6 and Table 3):

220 **Context #1: On the floors of small shield volcano summit pit craters.** We found four  
 221 such IMPs, namely Ina, Manilus-2, Cauchy-5 and #20 IMP in the Braden et al. (2014) catalog  
 222 (Figures 7A-D), and a possible one (Maskelyne) (Figure 7F). Three of the IMPs in this category,  
 223 Ina, Cauchy 5 and Maskelyne, are among the largest IMPs on the Moon, all with a maximum  
 224 length of ~3 km, suggesting that lunar shield-building eruptions and summit pit crater activities  
 225 may facilitate the development and emplacement of large IMPs (e.g., Strain & El-Baz, 1980;  
 226 Wilson & Head, 2017b; Qiao et al., 2019a). The other IMPs are much smaller, with a length  
 227 between ~200 and ~350 m, and are characterized by irregular shapes. The hosting shield  
 228 volcanoes are observed to vary in size and topography. The Ina shield volcano is ~22 km in base  
 229 diameter and ~320 m high (Figure 7A) and among the largest shield volcanos on the Moon  
 230 (Head & Gifford, 1980; Qiao et al., 2019a). The Cauchy-5 small shield volcano is ~5–6 km in  
 231 base diameter and ~40 m high. It also displays an elongate summit pit crater, ~0.75×2.5 km and  
 232 ~75 m deep (Figure 7B; Qiao et al., 2018b, 2020). The Manilus-2 small shield was previously  
 233 identified on telescopic photography and measured to be ~4.5 km in diameter (Head & Gifford,  
 234 1980); our updated measurement using Kaguya image and topography derives a ~5.0×5.5 km  
 235 base diameter and a ~80 m shield height (Figure 7D). New high-resolution image data also  
 236 resolve a summit pit crater which is ~0.7×0.5 km in diameter and ~30 m deep. The small shield  
 237 volcano that hosts the #20 IMP is newly-identified in this work. Kaguya TC DTM and  
 238 SLDEM2015 topography show that it is a circular dome structure, ~6×5 km in base diameter and

239 ~40 m high (Figure 7C). The flank of this shield is very gentle, with a kilometer-scale slope of  
240  $<1^\circ$ , explaining why it is not well resolved by image data and was not previously identified. The  
241 domical nature of the Maskelyne structure is suggested in low-sun angle images, with a base  
242 diameter of  $\sim 8.5 \times 6.5$  km, but is not well resolved on topography maps, as it is located on  
243 regional slopes and adjacent to several other domes (Figure 7F).

244 **Context #2: On the flanks of small shield volcanos.** Three IMPs are identified in this  
245 category, namely Cauchy-5 flank IMP (Figure 7B), Arago-5 IMP and Maclear-6 IMP (Figure  
246 7E). The Cauchy-5 small shield volcano hosts IMPs both on the summit pit crater floor (Context  
247 #1 IMP) and on the flank (Context #2 IMP) (Figure 7B). The Arago-5 (#9 IMP in the Braden et  
248 al. (2014) catalog) and Maclear-6 IMPs (newly identified IMP, Table 2) co-locate on different  
249 portions of the Arago-5 small shield (Figure 7E). The Arago-5 shield has been previously  
250 identified on telescopic photographs and measured to be 8 km in base diameter (Head & Gifford,  
251 1980). Updated Kaguya data-based morphometric and topographic investigation reveals the  
252 elliptical shape of this shield, oriented in a WNW direction, with a base diameter of  $\sim 7.7 \times 5.1$  km  
253 and  $\sim 90$  m height above the surrounding mare (Figure 7E). The summit pit crater is developed at  
254 the eastern part of this shield, which is  $\sim 1.6 \times 1.1$  km in diameter and  $\sim 180$  m lower than the pit  
255 rim, deeper than the mare surrounding the shield. IMP occurrences on the shield flanks are much  
256 smaller than those on the shield summit pit floor, with lengths less than 750 m.

257 **Context #3: Within linear/sinuuous rilles or pit crater chains.** Five IMPs are identified in  
258 this category, namely Sosigenes, Manilus-1, Hyginus IMP, Vera (newly identified; Table 2) and  
259 Nubium (Figure 8). Two of Context #3-type IMPs, Sosigenes and Nubium, are among the largest  
260 IMPs on the Moon, with lengths of 5 km and 2 km, respectively. The other three IMPs are much  
261 smaller, with lengths between  $\sim 70$  and  $\sim 270$  m. The pit craters that host these IMPs are observed  
262 to vary in morphology and tectonic setting, while all are plausibly interpreted to be atop dikes  
263 (see Head & Wilson, 2017). The elongate Sosigenes pit, co-aligned with a chain of pit craters, pit  
264 chains and linear ridges, may represent the collapse of the gas cavity at the dike-tip (Qiao et al.,  
265 2018a). The Hyginus crater,  $\sim 10$  km in diameter, occurs as a distinctive elbow in the  $\sim 215$ -km  
266 long graben system and is interpreted to be formed by surface subsidence into an evacuated sill  
267 developed at the dike tip (Wilson et al., 2011). The Vera IMP (Table 2) occurs within the source  
268 depression of Rima Prinz, which has been interpreted to be the source depression of a sinuous  
269 rille-forming volcanic eruption site (Hurwitz et al., 2012). The Nubium IMP occurs on the floor  
270 of an elongate rille that is  $\sim 4.7$  km long, up to  $\sim 1$  km wide and  $\sim 80$  m deep. The Manilus-1 IMP  
271 occurs on the floor of a depression that consists of two quasi-perpendicular rilles; the relatively  
272 larger rille, which also hosts larger IMPs, is  $\sim 1.2 \times 0.7$  km in size and up to  $\sim 55$  m deep.

273 **Context #4: On the rim or in the adjacent exterior of linear/sinuuous rilles.** Seven IMPs  
274 of this type are identified (Figure 9), namely the Nubium IMP (arrow in Figure 8B), #21, #45,  
275 #50, #63 (in the Braden et al. (2014) catalog), Aratus D-5 and Brayley D (Table 2). Among these  
276 IMPs, four occur at the upper wall or rim of linear rilles (#21, #45, Aratus D-5 and Brayley D  
277 IMPs) and three occur in the adjacent exterior mare surface of linear rilles (Nubium, #50 and #63  
278 IMPs), within a distance of up to  $\sim 1.7$  km from the rille rim. These associated linear rilles are  
279 observed to vary in size and depth. The Nubium IMP rille is  $\sim 4.2$  km long, up to  $\sim 1$  km wide and  
280 up to  $\sim 80$  m deep (Figure 8B). The linear feature associated with #21 IMP is about  $1.7 \times 0.4$  km in  
281 size and  $\sim 20$  m deep (Figure 9A), the smallest rille associated with IMPs in this category. The  
282 #45 and #50 IMPs are both associated with a huge linear rille in the east of Sinus Aestuum; the  
283 rille is  $\sim 90$  km long, typically 1–1.3 km wide and  $\sim 170$ – $270$  m deep (Figures 9B and C). The #50

284 IMP is also in the adjacent exterior mare surface of an elongate pit crater, which is 6.9×3.4 km in  
285 size and up to ~860 m deep (Figure 9C). The sinuous rille associated with #63 IMP is one of the  
286 rilles of the Rimae Prinz and is 38 km long, typically 1–1.5 km wide and up to 165 m deep (#66  
287 rille in the Hurwitz et al., (2013) list, Figure 9D). The associated rille of the Aratus D-5 IMP is  
288 ~6 km long, typical 0.4 km wide and up to ~70 m deep (Figure 9E). The Brayley D IMPs is  
289 associated with an elongate pit ~5.6 km long, typically 1.5–1.8 km wide and up to ~450 m deep  
290 (Figure 9F). The spatial distribution map of context #4 IMPs (Figure 6) indicates several ( $n = 5$ )  
291 of these IMPs appears to occur at the boundaries between maria and highlands. However,  
292 checking the local maps of these IMPs find they are still at a considerable distance from the mare  
293 boundary (ranging from ~5 to ~60 km), suggesting that basin-related tectonics and/or subsidence  
294 of mare basalts may not exert a dominant effect on the occurrence of lunar IMPs.

295 **Context #5: IMPs in typical mare deposits.** These can be further divided into two sub-  
296 categories:

297 **Context #5A: In relatively flat mare plain.** We have identified 47 IMPs in this subtype,  
298 making it the most common IMP type (Figure 10 and Table 3). The majority of Context #5A  
299 IMPs are associated with depressions within mare plains (mare pits) and are typically irregular  
300 and elongated in shape, similar to the many small pits observed on the Cauchy-5 shield flank  
301 (Figure 7B and Qiao et al., 2018b, 2020). The geologic settings of these IMP types are diverse in  
302 characteristics and can be further classified into several subtypes. Some IMPs occur at the  
303 bottom of depressions in the mare plain (Figures 10 A and I); these depressions are generally  
304 very shallow (generally less than ~5 m, measured from LROC NAC DTM topography; Figures  
305 10C and L), while some of them seem to be relatively deep (generally greater than ~10 m and up  
306 to ~40 m, measured from Kaguya TC DTM topography; Figures 10E, G and K). Some  
307 depressions are aligned in small pit chains (Figure 10D). These IMPs may occur at various  
308 locations in the associated depression. Some IMPs are present on the depression wall (Figures  
309 10H and J) and some IMPs occur on both the depression floor and wall slopes (Figure 10F).  
310 Several IMPs occur in mare plains that infill the floors of impact craters (Figure 10B).

311 **Context #5B: On typical mare features and structures.** We identified 26 IMPs in this  
312 category (Figure 11 and Table 3). As with Context #5A, IMPs in this subtype are also located  
313 within mare regions, but they occur locally on topographically raised mare features/structures  
314 (Figures 11B, D and I), or on the slopes of mare structures (Figure 3J). IMPs in this sub-type  
315 generally share context characteristics with Context #5A IMPs in mare plains, though their  
316 geologic settings are relatively less diversified. In a manner similar to Context #5A IMPs, many  
317 IMPs in this type also occur at the bottom of depressions in mare deposits; these associated  
318 depressions are generally very shallow (generally less than ~5 m, measured from Kaguya TC  
319 DTM topography; Figure 11C). No deep depressions (greater than ~10 m), such as those  
320 associated with Context #5A IMPs, are observed in this subtype. Also similar to Context #5A  
321 IMPs, some IMPs in this category occur on the walls and rims of depressions (Figures 3H and I),  
322 and the exterior ejecta deposit of some impact craters (Figure 11E). In addition, several IMPs of  
323 this type are located on mare ridges (Figure 11F). Context #5B IMPs are generally very small  
324 (dominantly 100–200 m in length, Figure 11H) and only a few are larger (up to 1.2 km in length,  
325 Figure 11A).

326 One of the most enigmatic features among the entire IMP population is the one ~25 km  
327 north of Aristarchus crater (25.044°N, 46.767°W; termed North Aristarchus IMP in the Braden  
328 et al. (2014) catalog). It seems to be located on the continuous ejecta deposit of Aristarchus

329 crater (Braden et al., 2014 and Figure 12A) and it is also very close (~2.7 km) to the mare  
 330 boundary mapped out by Nelson et al. (2014). Examination of high-resolution LROC NAC  
 331 imagery (Figure 12C) and topography (Figure 12D) shows that the clusters of small IMPs  
 332 forming this feature are actually located on local topographically high terrains, up to ~40–50 m  
 333 higher than the surrounding surface. Iron abundance mapping results (using Kaguya Multiband  
 334 Imager (MI) data and the Lemelin et al. (2015) algorithm) show that these topographic highs  
 335 have a FeO content >14 wt.%, comparable with that of the adjacent mare (Figure 12B),  
 336 indicating a basaltic composition for these terrains (either local mare basalts or distant mare  
 337 materials ejected by the Aristarchus impact). On the basis of these observations, we suggest that  
 338 the North Aristarchus IMP occurrences are located on mare features (possibly volcanic structures  
 339 mantled with thin Aristarchus ejecta) and can be classified as a Context #5B IMP.

## 340 **6. Characteristics and Classification**

341 We next examine the detailed characteristics of all the 91 documented IMP features using  
 342 high-resolution LROC NAC images, including structure, geomorphology, morphometry and  
 343 surface texture, and derive a classification scheme for IMP characteristics (Figures 13, 14 and  
 344 Table 3):

345 ***Characteristic class #1: Composed of a combination of positive-relief mounds and***  
 346 ***lower rough hummocky terrains (“mound + floor” type).*** Five IMPs are identified in this  
 347 category, namely Sosigenes, Ina, Cauchy-5 (summit pit floor and rim), Maskelyne and Nubium  
 348 (#1-5 IMPs in the Braden et al. (2014) catalog; Figures 14A-E). The five Class #1 IMPs are also  
 349 the largest IMPs among the entire IMP population, with lengths ranging from 2 to 5 km,  
 350 indicating that the building of the raised mounds requires a relatively high volume of lunar  
 351 volcanic materials. The mounds are characterized by a bleb-like and convex meniscus  
 352 appearance, and the lower hummocky units are characterized by ridged and pitted textures and  
 353 often host block exposures (e.g., Garry et al., 2012; Braden et al., 2014; Qiao et al., 2018a,  
 354 2019a).

355 ***Characteristic class #2: Composed of rough, bright pit terrains (“pit only” type).*** These  
 356 IMPs host pit terrains resembling the floor terrains in Class #1 IMPs, while lacking the  
 357 characteristic bleb-like raised mound structures. IMPs in this category are observed to occur in  
 358 various locations and can be further divided into two sub-categories:

359 ***Characteristic class #2A: “Pit only” IMPs within mare surface.*** We identify 65 IMPs in  
 360 the category, making it the most common characteristic sub-class of IMPs, including Cauchy-5  
 361 (shield flank, Figure 14C), Arago-5 (shield flank), Maskelyne (flank, Figure 14D), Maclear-2  
 362 IMP (Figure 14F), Aristarchus North IMP (Figure 14G), #22 IMP (Figure 14H), #35 IMP  
 363 (Figure 14I) and Hyginus IMP (Figure 14K).

364 ***Characteristic class #2B: “Pit only” IMPs associated with depressions (at the rim, wall***  
 365 ***or floor) or on slopes.*** 47 IMPs occurrences are classified into this sub-type, including Cauchy 5  
 366 flank (Figure 14C), Maskelyne (flank, Figure 14D), Aristarchus North IMP (Figure 14G), #35  
 367 IMP (Figure 14I), Manilus-2 (summit pit, Figure 14J), Hyginus IMP (Figure 14K) and #58 IMP  
 368 (Figure 14L). The depressions associated with Class #2B IMPs show variable characteristics and  
 369 origins. Many are characterized by a circular map view, bowl-shaped profile and raised rim crest  
 370 (Figures 14C and L), revealing that these depressions are typical small impact craters. Some  
 371 associated depressions are characterized by irregular shapes and cross-section profiles (e.g.,

372 Figures 3H, 14G, I and L), which probably represent collapse depressions of several types, like  
373 drainage pits. At two IMP occurrences, the associated depressions are probably endogenetic in  
374 origin: the Manilus-2 IMP depression occurs as a summit pit of a small shield volcano (Figures  
375 7D and 14J) and the #45 IMP occurs on the interior wall and rim of a long linear rille (Figure  
376 9B). Various sub-types of associated depressions are also accompanied by characteristic spatial  
377 distribution patterns of the IMP occurrences. In the impact crater case, the IMPs are often around  
378 the upper inner wall, hinting at their formation below the surface of the pre-impact mare and  
379 revealing a layer of unusual properties (probably highly vesicular basalt; Wilson & Head, 2017b;  
380 Qiao et al., 2019a) exposed by the impact. In the collapse depression case, it is possible that a  
381 large collapse depression formed over an area of magmatic gas voids or possibly a buried crater,  
382 where the formation of gas might have been enhanced by the locally thicker lava.

### 383 6.1 Surface Textures of the Floor Terrains of Lunar IMPs

384 The various types of IMP occurrences share a lot of similarities, but also show many  
385 differences: both the lower hummocky units of Class #1 IMPs and pit terrains of Class #2 IMPs  
386 are characterized by complicated surface textures, including blocky, ridged and vermicular  
387 terrains, but the Class #2 IMPs lack the characteristic mound terrains observed at Class #1 IMPs.  
388 We use our prior detailed characterization of Ina floor terrain surface textures as a frame of  
389 reference (Qiao et al., 2019a: section 3.5 and Figure 13) and survey the detailed textures of other  
390 IMP occurrences (floor hummocky terrains of Class #1 IMPs and pit terrains of Class #2 IMPs;  
391 Table 3). Surface textures of Ina floor terrains include: (1) relatively smooth texture, (2)  
392 hummocky texture, (3) pitted texture, (4) ridged texture, (5) polygonal texture, (6) vermicular  
393 texture and (7) blocky texture (Figures 15A and B). Additional texture subtypes observed at  
394 other IMP occurrences are (8) uneven texture and (9) bright streak (Figure 15C): uneven textures  
395 are characterized by rough and coarse morphology, while lacking the small domical structures of  
396 the hummocky textures; and bright streaks are characterized by elongations downslope,  
397 relatively higher albedo than their surroundings and no detectable topographic relief. Various  
398 types of floor terrain textures often co-occur at one single IMP (Table 3). The statistic histogram  
399 of texture type occurrence shows that the hummocky, pitted, blocky and uneven textures are the  
400 most common types of textures, which are present (either occur alone or co-occur) at almost all  
401 IMPs (Figure 15D).

402 We also employ the LROC NAC DTM topography-derived slope maps to characterize the  
403 topographic slope of the various surface textures of the IMP floor terrains (Figure 15E). We find  
404 that the slopes of the various texture types do not correspond exactly to their morphological  
405 patterns, as the same type of texture may have a range of topographic slopes and various kinds of  
406 textures may have comparable slopes. We attribute this disparity to the contrasting  
407 resolution/baseline of the source data from which the morphology and topographic slope are  
408 interpreted: the morphology is derived from LROC NAC images with a typical pixel size of ~0.5  
409 m and the topographic slope map is calculated at a baseline of 6 m (2 m/pixel NAC DTM) or 15  
410 m (5 m/pixel NAC DTM); the dimension of many textures of IMP floor terrains (for instance,  
411 hummocky and pitted features) are, however, just between the LROC NAC pixel size and slope  
412 map baseline, making them observable on NAC images, but unidentifiable on slope maps.  
413 However, comparison of the slope measurements still shows apparent differences between the  
414 various surface texture patterns. Smooth and uneven textures are characterized by the smallest  
415 slopes (though with a relatively wide slope range due to the aforesaid baseline effect); this is  
416 evidenced by their observed relatively simple texture and relief. Hummocky, pitted, ridged and

417 polygonal texture types are observed to all have comparable slopes to those of the smooth  
418 textures ( $\sim 3\text{--}6^\circ$ ), though they have much more complicated and differentiated surface textures  
419 than the latter from NAC images, which can be explained by the fact that most of these texture  
420 units are shorter than the slope baseline. The vermicular textures are characterized by a slightly  
421 elevated slope ( $\sim 6.5^\circ$ ), which is attributed to the observed much larger size of these vermicular  
422 structures (larger than the ridged units and slope baseline). The blocky textures have even steeper  
423 slopes (typically  $\sim 10^\circ$ ); this is consistent with their observed rugged appearance, topography and  
424 position (often in the topographical moats surrounding the mound terrains). The bright streak  
425 textures are characterized by the steepest slope (typically  $>10^\circ$ ) among all the observed floor  
426 terrain texture types, as they mainly occur on the slopes of volcanic structures.

## 427 **7. Discussion**

### 428 7.1 Association between the Sizes, Geologic Contexts and Characteristics of Lunar IMPs

429 The IMP populations in various geologic context and characteristic categories are observed  
430 to have quite different dimensions (Figures 16A and B). One of the main observations is the  
431 distinctly larger size of lunar IMPs in Context #1 (within shield summit pits, median length 2.5  
432 km and maximum length 3 km) and #3 (within other endogenetic pits, median length 270 m and  
433 maximum length 5 km) than other IMPs (Figure 16A), indicating that the geologic settings of  
434 being contained within a pit crater may be the key factor for the development and emplacement  
435 of large IMPs. However, several IMPs in these two context categories are also relatively smaller  
436 (70–350 m in length), showing that being contained within a depression does not ensure the  
437 development of large IMPs and additional factors are involved. In these two characteristic  
438 classes of lunar IMPs, Class #1 IMPs (“mounds + floor” type, median length 2.6 km and  
439 maximum length 5 km) are just the top five largest IMPs among the entire IMP catalogue and are  
440 overwhelmingly larger than IMPs in any other category (“pit only” type; Figure 16B), suggesting  
441 the requirement of large volumes of building materials for the development of the raised  
442 mounded terrains.

443 The entire IMP population also shows subtle associations between the classification scheme  
444 in terms of the geologic context and the characteristics (Figure 16C). The special Class #1 IMPs  
445 with distinctive mound terrains (“mound + floor” type) exclusively occur within volcanic pit  
446 craters (Context #1 and #3), illustrating a close link between the geologic context (being  
447 contained within a pit crater) and the evolution of lunar IMP-formation process (emplacement of  
448 uplifted mound terrains). These IMPs are also among the largest and best-studied IMPs (e.g.,  
449 Strain & El-Baz, 1980; Schultz et al., 2006; Garry et al., 2012; Braden et al., 2014; Qiao et al.,  
450 2017, 2018a, 2019a, 2020). The “pit only” type IMPs (Class #2) mostly occur on mare regions  
451 (Context #5A and #5B), suggesting another important association between mare context and the  
452 origin of small IMP occurrences. In addition, the two IMP clusters, “mound + floor” type and  
453 “pit only” type, co-occur at three IMP features (Cauchy-5, Maskelyne and Nubium), some of  
454 which show clear geologic setting links between the two IMP populations (especially the IMPs at  
455 the Cauchy-5 summit pit and flank, Qiao et al., 2018b, 2020), showing a promising potential for  
456 relating the origin of the two IMP populations.

### 457 7.2 Implications of the Classification Scheme Results for Models of Origin of Lunar IMPs

458 Although specific detailed studies are needed for each of the individual occurrences of  
459 IMPs, the updated classification scheme, and the insights provided by sub-classification guided

460 by geologic context and IMP internal characteristics, provide new insights and directions for  
461 future research. Specifically, of the six hypotheses previously proposed for the origin of lunar  
462 IMPs (Table 1), the diversity of environments, settings and characteristics outlined here suggests  
463 that single process models, such as sublimation (Whitaker, 1972), pyroclastic eruptions (Carter et  
464 al., 2013) and removal of surface regolith by episodic out-gassing within the past 10 Ma (Schultz  
465 et al. 2006) are insufficient to account for the wide range of observations. Instead, more complex  
466 processes, involving several stages and geologic processes, appear to be more likely. For  
467 example, the geologic context of occurrences associated with volcanic vents (e.g., floors of pit  
468 craters on the summits of small shield volcanoes; interior of sinuous rille source depressions) and  
469 volcanic constructs (the rim and flanks of small shield volcanoes; the rim of sinuous rille source  
depressions) both point to volcanic processes operating in the source region.

471 Their preservation in the relatively youngest deposits in the specific occurrences also favors  
472 modes of origin that operate in the later stages of the evolution of vents and associated eruptions.  
473 Thus, new developments in understanding the sequence of stages in lunar mare basalt eruptions  
474 (e.g., Wilson & Head, 2018) may provide insights into a wider range of temporal behavior  
475 (particularly volatile release patterns) in observed lunar volcanic eruptions and the IMPs. For  
476 example, the association with final-stage activity in closely related vent areas such as shield  
477 volcano summit pit craters would seem to favor proposed origins such as small lava intrusions  
478 within a collapse caldera atop an extrusive volcanic dome (e.g., El-Baz, 1972, 1973; Strain & El-  
479 Baz, 1980), lava flow inflation (e.g., Garry et al., 2012) or lava lake processes and magmatic  
480 foam extrusion (e.g., Qiao et al, 2017, 2018a, 2019a; Wilson & Head 2017b).

481 In addition, the close association of these IMP contexts with ancient volcanic edifices (>3  
482 Ga) raises the question of why the CSFD ages of the major IMPs point to ages of <0.1 Ga  
483 (Braden et al., 2014), and suggest that alternate explanations should be investigated to account  
484 for the apparently abnormally young CSFD ages that occur in close geologic association with  
485 features formed over 3 Ga earlier.

486 Finally, the geologic context of small IMPs as isolated occurrences associated with ancient  
487 lunar mare deposits, initially reported by Braden et al. (2014) and reiterated here with our larger  
488 IMP population, provides new insights into IMP origins, and directions for further research. The  
489 classification reported here underlines the characteristics of these small IMP occurrences and  
490 shows that they are dominated by deposits analogous to the rough floor unit in the larger  
491 occurrences, with only minor occurrences of the distinctive mound units seen in the larger  
492 examples. This suggests that the optical immaturity of the small IMP occurrences may be related  
493 to drainage into subsurface voids, a process that could occur due to subsequent superposed  
494 impact craters over billions of years following the initial emplacement of the flows. Such voids  
495 might be related to the latter stages of lava flow emplacement several billion years ago in which  
496 flow inflation and second boiling might occur, creating subsurface void spaces and macro-  
497 vesicular substrates (e.g., Wilson & Head, 2017b, 2018) susceptible to subsequent collapse due  
498 to superposed impacts.

499 On the basis of (1) our previous theoretical treatment and observational investigation of the  
500 formation mechanism of several representative lunar IMPs (including Ina, Sosigenes and  
501 Cauchy-5; Wilson & Head, 2017b; Qiao et al., 2017, 2018a, 2019a, 2020) and (2) the new  
502 classification scheme presented here, we address that the described waning-stage magmatic foam  
503 formation and extrusion scenario is also applicable to the origin of lunar IMPs of various classes

504 catalogued in this study and the wide range of observed characteristics can be largely explained  
505 in this eruptive context.

506 Guided by the documented features at representative lunar IMPs, especially Ina and  
507 Cauchy-5 (Qiao et al., 2019a, 2020), we find that the various geologic contexts of lunar IMPs  
508 (Context #1-5 in section 5) can be generally grouped into two major categories: (1) pit crater  
509 environment (Context #1 and #3; being contained within a pit crater, or closed environment) and  
510 (2) (near-vent) mare flow environment (Context #2, #4, and #5; not being contained with a pit  
511 crater, simply emplaced on maria, or open environment).

512 In the pit crater environment, upwelling magma in the waning stages of the eruption would  
513 accumulate within the pit crater and formed a lava pond. Decrease of the magma ascent rate to  
514 less than  $\sim 1$  m/s favored gas bubble (mainly CO) production and coalescence, initiating a  
515 strombolian activity phase. This phase would deform, disrupt and fracture the cooling lava lake  
516 crust; a solidified lava lake crust characterized by abundance vesicularity and macro-porosity  
517 would be the resultant deposits (the lower rough and hummocky terrains of Class #1 IMPs). In  
518 the final stage of the eruption, the magma rise rate had become negligible and no additional  
519 magma would ascent from depth, H<sub>2</sub>O gas exsolution produced viscous magmatic foam with an  
520 extreme vesicularity up to  $\sim 95\%$  below the chilled lake crust. The final-stage dike closure caused  
521 the foamy magma extruded out onto the rough pit crater floor crust to produce the bleb-like  
522 raised mounds (the mound terrains of Class #1 IMPs). This formation scenario is consistent with  
523 our observations that all Class #1 IMPs are located in pit crater environments (Context #1 and  
524 #3, Figure 16B). Only in this context of being contained within a pit crater, the extruded  
525 magmatic foams can be potentially thick enough to build up the large (much larger than IMPs of  
526 other categories; Figure 16A) and raised mound terrains. However, being contained within a pit  
527 crater does not assure the development of raised mounds, as the extruded waning-stage magma  
528 foam can be simply not voluminous enough to do that, consistent with the occurrences of several  
529 Class #2 “pit only” IMPs in pit crater environments (Figure 16B).

530 In the (near-vent) mare flow environment, instead of being contained by a summit pit crater  
531 or collapse crater and forming a lava lake, the final-stage, very vesicular and foamy magma  
532 would exit the fissure vent and overflow onto the adjacent surface beyond the vent rim  
533 (including shield flanks (Context #2) and the exterior of volcanic rilles (Context #4)) or spread  
534 out across the maria (Context #5) as a cooling and meters-thick foamy lava flows (Qiao et al.,  
535 2020). Subsequent meteoritic impacts into the emplaced foamy flows caused collapse of voids of  
536 various scales and shapes. Collapse in the foamy lavas was likely to expose the fresh and more  
537 coherent interior of the void-rich flows at the depression floor and/or upper walls, consistent with  
538 the observed bright and rough textures of the pit terrains of Class #2 IMPs (section 6 and Figure  
539 14). The high porosity and inhomogeneous substrate properties of the foamy flows resulted in  
540 the post-emplacment crater formation and impact-derived collapse process to be very atypical  
541 and complicated, generating the irregular crater appearance and various surface textures of the  
542 floor terrains of lunar IMPs (hummocky, pitted, blocky, uneven, etc.; section 6.1 and Figure 15).  
543 Some of the extruded foamy lava might flow and emplace on topographically raised terrains  
544 (including mare structures and mare ridges for Context #5B IMPs) or sloped surface, impact-  
545 derived collapse of these flows would potentially result in the observed “bright streak” surface  
546 texture patterns at the pit terrains of several small Class #2 IMPs (section 6.1).

547 7.3 Outstanding Unanswered Questions

548 The origin of lunar IMPs is one of most debated topics of lunar volcanism and geological  
549 evolution history. The formation age, emplacement mechanism, evolution during the formation  
550 process, properties of the resultant deposits, and post-emplacement modification and its effect on  
551 the current observations represent key parts of any IMP origin model. The different and  
552 competing theories for their origin have already raised a list of outstanding questions about lunar  
553 IMPs (Table 1). Our new classification scheme in terms of the geologic settings and  
554 characteristics of lunar IMPs has contributed to address some of these key questions concerning  
555 the origin of lunar IMPs (section 7.2), but it also specifically introduces a second set of  
556 outstanding questions that adds to and complements the first set of questions, each meriting  
557 further investigations:

558 (1) *Why are lunar IMPs so uncommon in the lunar maria?* The vast majority of lunar IMPs,  
559 especially smaller pit-type IMPs (Class #2), are found in lunar maria. But only a very small  
560 percent of stratigraphically-defined mare units ( $17/482 = 3.5\%$ , section 4) host lunar IMPs and  
561 no IMPs have been identified on lunar farside maria. If low effusion rates and foam buildup are  
562 typical of each mare volcanic eruption (e.g., Wilson & Head, 2017a, 2018), then why don't we  
563 see lunar IMPs everywhere? It is possible that even the most common mare deposit-forming  
564 eruptions may also operate in very different phases and styles, and lead to widely varying  
565 resultant deposits, modulated by a range of factors including effusion rates, eruption durations,  
566 cooling and supply limitations to flow length, and pre-existing topography (Head & Wilson,  
567 2017). Our recent theoretical treatments of lunar basaltic volcanic eruptions suggested that gas  
568 release patterns and vesiculation processes are especially crucial in determining the final  
569 resultant disparate volcanic deposits including lunar IMPs (Wilson & Head, 2018). Lunar IMPs-  
570 hosting maria are probably formed by volcanic eruptions defined by a narrow parameter space.  
571 Theoretical and observational analyses of mare volcanism and the final-stage volatile exsolution  
572 physics will provide an important framework for revealing the formation environment and  
573 evolution of lunar IMPs.

574 (2) *Why are IMPs so uncommon in small lunar shield volcano pit crater floors?* Lunar  
575 small shield volcano summit pit floors are one of the common geologic settings of IMPs and host  
576 some of the most prominent examples, including Ina and Cauchy-5. Small shield volcanos are  
577 common on the Moon. Over 300 small shields have been identified and dozens of them  
578 developed summit pit craters (e.g., Head & Gifford, 1980; Tye & Head, 2013). However, only  
579 five small shield pit crater floors host IMP features (Figure 7). These observations raise a line of  
580 questions concerning lunar shield-building eruptions, summit pit activities and the resultant  
581 deposits. What are the detailed morphologies of all small shield volcano pits and their variations?  
582 What do their flanks look like? What are the roles and effects of the total volume of involved  
583 magma and the behavior of waning-stage pit crater processes (a combination of extrusion of  
584 foams from below the lava crust, drain back, cooling and thermal contraction, monotonic or  
585 punctuated decline in the final effusion rates, etc.)? Each of these questions deserves further  
586 analyses. A general survey of global lunar small shield volcanoes has not been conducted since  
587 the preliminary analyses in 1980 that employed nearly half-century-old imagery sets (Lunar  
588 Orbiter, Apollo, etc.), which already showed that lunar small shields varied widely in geologic  
589 settings, association with other features, outlines, base diameters, cross-sectional shapes, summit  
590 craters (presence or absence, dimension). These initial observations indicate contrasting  
591 processes in their formation and evolution (Head & Gifford, 1980) and it is possible that the  
592 IMP-related shield volcanoes are formed under very particular eruption conditions. In addition,  
593 the detailed topography, morphology and texture of the summit pit and flank have yet to been

594 examined in details due to the lack of images and topography data of sufficient resolution in  
595 prior investigations. The newly-acquired sub-meter scale LROC NAC images and high-precision  
596 LOLA altimetric measurements will provide an unprecedented opportunity for such  
597 investigations. Moreover, a detailed compositional analysis of the entire population of lunar  
598 IMPs and small shield volcanos could also help answer this outstanding question.

599 (3) *What are the implications of these associations and characteristics for the debate about*  
600 *the age of IMPs?* The emplacement age of lunar IMPs is one of the most debated topics of lunar  
601 geosciences (e.g., Stopar et al., 2019). Prevailing ideas include outgassing removal of surface  
602 regolith within the past 10 Ma (Schultz et al. 2006), geologically very recent (within the past 100  
603 Ma) small volcanic eruptions (Braden et al., 2014) and ancient ( $> 3$  Ga) volcanism producing  
604 highly vesicular deposits (Qiao et al., 2019a). We suggest that the age of the host mare units  
605 (Figures 4B and 5) and the geologic settings (Figure 6) can provide instructive information on  
606 determining the formation and age of lunar IMPs: Interpretation for the formation mechanism  
607 and age of the IMPs must incorporate the facts that the vast majority of lunar IMPs are located in  
608 ancient mare volcanic deposits. Determining the age of lunar IMPs will provide direct key  
609 constraints on the cessation time of lunar volcanism ( $< 100$  Ma or  $\sim 1$  Ga?) and strengthen our  
610 knowledge of lunar geologic and thermal evolution history, including the current thermal status  
611 of the lunar interior, the inventory of lunar heat-producing elements, and the global stress state  
612 field of the lunar lithosphere.

613 (4) *How is our understanding of lunar IMPs limited by the current observations and what*  
614 *new measurements from future exploration missions would unambiguously answer these*  
615 *questions?* We address that the current limitations on the nature and origin of lunar IMPs include  
616 the quantitative physical properties, microstructures (e.g., small fractures) and porosity of IMP  
617 deposits (mound and floor terrains), shallow subsurface structure and properties, and the detailed  
618 impact cratering mechanism in highly porous targets and the resultant effects on crater retention  
619 age estimations. Needed new measurements from future exploration endeavors include: (a)  
620 Orbital missions: dedicated high-resolution photometric and/or polarimetric measurements to  
621 constrain the micro-structure (including sub-resolution roughness and particle sizes) of the  
622 surface of lunar IMPs, for instance, the Wide-Angle Polarimetry Camera (PolCam) to fly on the  
623 forthcoming Korea Pathfinder Lunar Orbiter (Sim et al., 2019); (b) Landed missions: cameras,  
624 microscopic imagers, seismometers, penetrometers and other geophysical instruments to  
625 determine the surface and shallow subsurface physical properties and structures (e.g., the  
626 Irregular Mare Patch Exploration Lander (IMPEL) mission concept (Draper et al., 2018)), and  
627 in-situ radiometric dating measurements to determine the crystallization age of IMP deposits, for  
628 example, the Chemistry, Organics, and Dating EXperiment (CODEX) mission concept  
629 (Anderson et al., 2017); (c) Sample return missions: providing direct and high-precision  
630 radiometric dates, petrography, chemical and isotopic compositions for the deposits of lunar  
631 IMPs, readily distinguishing their crystallization age and deposition mechanism. In addition,  
632 laboratory and numerical simulation experiments on the detailed impact cratering mechanism in  
633 highly porous targets and the resultant effects on crater retention ages would also contribute to  
634 uncover the formation age and post-emplacement evolutions of lunar IMPs.

## 635 **8. Conclusions**

636 We compiled all previous lunar IMP identifications since the Apollo era and present an  
637 updated, comprehensive inventory of 91 lunar IMPs, which expands the known IMP occurrences

638 into two additional nearside maria: Mare Serenitatis and Mare Imbrium. The ages of the maria  
639 hosting lunar IMPs are documented and show that the majority occur in mare units emplaced  
640 more than three billion years ago, contemporaneous with the climax of global lunar volcanism,  
641 suggesting that alternate formation mechanisms of lunar IMPs should be investigated in  
642 reference to their apparently abnormally young CSFD ages. We then surveyed the detailed  
643 geological characteristics of each IMP feature using the latest high-resolution image and  
644 altimetric data sets and derived classification schemes for all catalogued IMPs in terms of their  
645 geologic settings and characteristics. The entire lunar IMP population is observed to occur in a  
646 range of geologic settings, which are categorized into small shield volcano summit pit floor  
647 (Context #1) and flank (Context #2), pit crater chain or linear/sinuuous rille interior (Context #3)  
648 and adjacent exterior (Context #4) and typical mare deposits (Context #5A: mare plain and  
649 Context #5B: mare volcanic edifices). The characteristics and structure of IMPs themselves were  
650 classified into “mound + floor” type (Class #1) and “pit only” type (Class #2A: within maria and  
651 Class #2B: associated with depressions). Our updated catalogue and new classification scheme  
652 of lunar IMPs showed that the wide range of geologic settings and characteristics were consistent  
653 with the waning-stage magmatic foam formation and extrusion scenario in different  
654 environments: (1) in the pit crater environment (Context #1 and #3), waning-stage lava lake  
655 magmatic foam extrusions within the pit crater produced magmatic foam deposits (the mound  
656 terrains of Class #1 IMPs) superposed on the chilled lava lake crust (the lower hummocky  
657 terrains of Class #1 IMPs); (2) in the (near-vent) mare flow environment (Context #2, #4 and  
658 #5), impacts into the overflowed thin foamy flows across the maria resulted in void collapse,  
659 exposing the fresh and coherent interior of the solidified magma foams (rough and bright pit  
660 terrains of Class #2 IMPs). In addition, our newly presented lunar IMP catalog and classification  
661 schemes also raise a list of outstanding questions concerning the nature and formation  
662 mechanism of lunar IMPs. Assessing these questions will solidify our knowledge of lunar  
663 thermal and geological evolution history.

## 664 **Acknowledgements**

665 This study is supported in part by the National Natural Science Foundation of China (No.  
666 41703063, 11941001 and 41972322), a Pre-research Project on Civil Aerospace Technologies  
667 No. D020205 funded by CNSA, the grant from Key Laboratory of Lunar and Deep Space  
668 Exploration, CAS (No. LDSE201902), the China Postdoctoral Science Foundation (Nos.  
669 2017M610421 and 2018T110682) and the Natural Science Foundation of Shandong Province  
670 (ZR2019MD008). J. W. H. gratefully acknowledge financial support from the NASA Lunar  
671 Reconnaissance Orbiter Lunar Orbiter Laser Altimeter (LOLA) experiment (grants  
672 NNX09AM54G and NNX11AK29G) and the NASA Solar System Exploration Research Virtual  
673 Institute (SSERVI) grant for Evolution and Environment of Exploration Destinations under  
674 cooperative Agreement No. NNA14AB01A at Brown University. L. W. thanks the Leverhulme  
675 Trust for support via an Emeritus Fellowship. We thank the Editors Laurent Montesi and David  
676 Baratoux and the reviewers for their very helpful comments. All original Lunar Orbiter  
677 photographs can be retrieved from the Lunar Orbiter Digitization Project  
678 (<https://astrogeology.usgs.gov/Projects/LunarOrbiterDigitization/>), all original Apollo  
679 photographs can be found at the Apollo Image Archive (<http://apollo.sese.asu.edu/index.html>),  
680 all original LRO data (LROC, LOLA and SLDEM2015) are accessible at the PDS Geosciences  
681 Node (<https://pds-geosciences.wustl.edu/missions/lro/default.htm>) and all original  
682 Kaguya/SELENE TC and MI data are archived at SELENE Data Archive

683 (<https://darts.isas.jaxa.jp/planet/pdap/selene/>). The updated IMP catalogue and slope  
 684 measurements of the various surface textures are accessible at Zenodo  
 685 (<https://zenodo.org/record/3772253>).

## 686 **References**

- 687 Anderson, F. S., Whitaker, T. J., Wiesendanger, R., Wurz, P., Beck, S., & Levine, J. (2017).  
 688 Revealing lunar history with CODEX: Miniature mass spectrometer Rb-Sr results. *5th*  
 689 *European Lunar Symposium*, University of Münster, Münster, Germany, 25-26.
- 690 Anderson, J. A., Sides, S. C., Soltész, D. L., Sucharski, T. L., & Becker K. J. (2004).  
 691 Modernization of the integrated software for imagers and spectrometers. *35th Lunar and*  
 692 *Planetary Science Conference*, Lunar and Planetary Institute, League City, Texas, abstract  
 693 #2039.
- 694 Barker, M. K., Mazarico, E., Neumann, G. A., Smith, D. E., & Zuber, M. T. (2014). Merging  
 695 digital elevation models from the Lunar Orbiter Laser Altimeter and Kaguya Terrain Camera.  
 696 *45th Lunar and Planetary Science Conference*. Lunar and Planetary Institute, The Woodlands,  
 697 Texas, abstract #1635.
- 698 Barker, M. K., Mazarico, E., Neumann, G. A., Zuber, M. T., Haruyama, J., & Smith, D. E.  
 699 (2016). A new lunar digital elevation model from the Lunar Orbiter Laser Altimeter and  
 700 SELENE Terrain Camera. *Icarus*, 273, 346-355. <https://doi.org/10.1016/j.icarus.2015.07.039>
- 701 Bennett, K. A., Horgan, B. H. N., Bell, J. F., III, Meyer, H. M., & Robinson, M. S. (2015). Moon  
 702 Mineralogy Mapper investigation of the Ina irregular mare patch. *46th Lunar and Planetary*  
 703 *Science Conference*, Lunar and Planetary Institute, The Woodlands, Texas, abstract #2646.
- 704 Braden, S. E. (2013). Analysis of spacecraft data for the study of diverse lunar volcanism and  
 705 regolith maturation rates (Doctoral dissertation). Retrieved from ASU Library.  
 706 (<http://repository.asu.edu/items/20943>). Tempe, AZ: Arizona State University.
- 707 Braden, S. E., Stopar, J. D., Robinson, M. S., Lawrence, S. J., van der Bogert, C. H., &  
 708 Hiesinger, H. (2014). Evidence for basaltic volcanism on the Moon within the past 100 million  
 709 years. *Nature Geoscience*, 7(11), 787-791. <https://doi.org/10.1038/ngeo2252>
- 710 Bowman-Cisneros, E. (2010). *LROC EDR/CDR Data Product Software Interface Specification*.  
 711 Retrieved from [http://lroc.sese.asu.edu/data/LRO-L-LROC-2-EDR-](http://lroc.sese.asu.edu/data/LRO-L-LROC-2-EDR-V1.0/LROLRC_0001/DOCUMENT/LROCSIS.PDF)  
 712 [V1.0/LROLRC\\_0001/DOCUMENT/LROCSIS.PDF](http://lroc.sese.asu.edu/data/LRO-L-LROC-2-EDR-V1.0/LROLRC_0001/DOCUMENT/LROCSIS.PDF)
- 713 Carter, L. M., Hawke, B. R., Garry, W. B., Campbell, B. A., Giguere, T. A., & Bussey, D. B. J.  
 714 (2013). Radar observations of lunar hollow terrain. *44th Lunar and Planetary Science*  
 715 *Conference*, Lunar and Planetary Institute, The Woodlands, Texas, abstract #2146.
- 716 Cho, Y., Morota, T., Haruyama, J., Yasui, M., Hirata, N., & Sugita, S. (2012). Young mare  
 717 volcanism in the Orientale region contemporary with the Procellarum KREEP Terrane (PKT)  
 718 volcanism peak period ~2 billion years ago. *Geophysical Research Letters*, 39(11).  
 719 <https://doi.org/10.1029/2012GL051838>
- 720 Donaldson Hanna, K. L., Evans, R., Bowles, N. E., Schultz, P. H., Greenhagen, B. T., & Bennett,  
 721 K. A. (2016). Investigating young (<100 million years) irregular mare patches on the Moon  
 722 using diviner observations. *47th Lunar and Planetary Science Conference*, Lunar and  
 723 Planetary Institute, The Woodlands, Texas, abstract #2127.
- 724 Draper, D. S., Stopar, J. D., Lawrence, S. J., Denevi, B., John, K., Graham, L., et al. (2018), The  
 725 Irregular Mare Patch Exploration Lander (IMPEL) SmallSat mission concept. *49th Lunar and*  
 726 *Planetary Science Conference*, Lunar and Planetary Institute, The Woodlands, Texas, abstract  
 727 #1617.

- 728 El-Baz, F. (1972). New geological findings in Apollo 15 lunar orbital photography. *Proceedings*  
729 *of 3rd Lunar and Planetary Science*, 39–61.
- 730 El-Baz, F. (1973), D-caldera: New photographs of a unique feature. In *Apollo 17 Preliminary*  
731 *Science Report* (NASA SP-330, pp. 30-13–30-17). Washington, DC: United States  
732 Government Printing Office.
- 733 Elder, C. M., Hayne, P. O., Bandfield, J. L., Ghent, R. R., Williams, J. P., Donaldson Hanna, K.  
734 L., & Paige, D. A. (2017). Young lunar volcanic features: Thermophysical properties and  
735 formation. *Icarus*, 290, 224-237. <https://doi.org/10.1016/j.icarus.2017.03.004>
- 736 Evans, R. E., & El - Baz, F. (1973), Geological observations from lunar orbit. In *Apollo 17*  
737 *Preliminary Science Report* (NASA SP-330, pp. 28-1–28-32). Washington, DC: United States  
738 Government Printing Office.
- 739 Garry, W., Robinson, M., Zimbelman, J., Bleacher, J., Hawke, B., Crumpler, L., et al. (2012),  
740 The origin of Ina: Evidence for inflated lava flows on the Moon, *Journal of Geophysical*  
741 *Research: Planets*, 117, E00H31. <https://doi.org/10.1029/2011JE003981>
- 742 Garry, W. B., Hawke, B. R., Crites, S., Giguere, T., & Lucey, P. G. (2013). Optical maturity  
743 (OMAT) of Ina 'D-Caldera', the Moon. *44th Lunar and Planetary Science Conference*, Lunar  
744 and Planetary Institute, The Woodlands, Texas, abstract #3058.
- 745 Glaspie, L. M., Bennett, K. A., Gaddis, L. R., Donaldson Hanna, K. L., Horgan, B. H. N.,  
746 Keszthelyi, L., et al. (2019). Characterization of a potential compositional halo around Ina  
747 irregular mare patch. *50th Lunar and Planetary Science Conference*, Lunar and Planetary  
748 Institute, The Woodlands, Texas, abstract #2889.
- 749 Grice, J. P., Donaldson Hanna, K. L., Bowles, N. E., Schultz, P. H., & Bennett, K. A. (2016).  
750 Investigating young irregular mare patches on the Moon using Moon Mineralogy Mapper  
751 observations. *47th Lunar and Planetary Science Conference*, Lunar and Planetary Institute,  
752 The Woodlands, Texas, abstract #2106.
- 753 Haruyama, J., Matsunaga, T., Ohtake, M., Morota, T., Honda, C., Yokota, Y., et al. (2008).  
754 Global lunar-surface mapping experiment using the Lunar Imager/Spectrometer on SELENE.  
755 *Earth, Planets and Space*, 60(4), 243-255. <https://doi.org/10.1186/BF03352788>
- 756 Haruyama, J., Ohtake, M., Matsunaga, T., Morota, T., Honda, C., Yokota, Y., et al. (2009).  
757 Long-lived volcanism on the lunar farside revealed by SELENE Terrain Camera. *Science*,  
758 323(5916), 905. <https://doi.org/10.1126/science.1163382>
- 759 Haruyama, J., Hara, S., Hioki, K., Iwasaki, A., Morota, T., Ohtake, M., et al. (2012). Lunar  
760 global digital terrain model dataset produced from SELENE (Kaguya) terrain camera stereo  
761 observations. *43rd Lunar and Planetary Science Conference*, Lunar and Planetary Institute,  
762 The Woodlands, Texas, abstract #1200.
- 763 Head, J., & Gifford, A. (1980). Lunar mare domes: Classification and modes of origin. *The*  
764 *Moon and the Planets*. 22, 235-258. <https://doi.org/doi:10.1007/BF00898434>
- 765 Head, J. W., & Wilson, L. (2017). Generation, ascent and eruption of magma on the Moon: New  
766 insights into source depths, magma supply, intrusions and effusive/explosive eruptions (Part 2:  
767 Predicted emplacement processes and observations). *Icarus*, 283, 176-223.  
768 <https://doi.org/10.1016/j.icarus.2016.05.031>
- 769 Henriksen, M. R., Manheim, M. R., Burns, K. N., Seymour, P., Speyerer, E. J., Deran, A., et al.  
770 (2017). Extracting accurate and precise topography from LROC narrow angle camera stereo  
771 observations. *Icarus*, 283, 122-137. <https://doi.org/10.1016/j.icarus.2016.05.012>
- 772 Hiesinger, H., Head, J. W., III, Wolf, U., Jaumann, R., & Neukum, G. (2006). New ages for  
773 basalts in Mare Fecunditatis based on crater size-frequency measurements. *37th Lunar and*

- 774 *Planetary Science Conference*. Lunar and Planetary Institute, The Woodlands, Texas, abstract  
775 #1151.
- 776 Hiesinger, H., Head, J. W., Wolf, U., Jaumann, R., & Neukum, G. (2011a). Ages and  
777 stratigraphy of lunar mare basalts: A synthesis. *Geological Society of America Special Papers*,  
778 477, 1-51. [https://doi.org/10.1130/2011.2477\(01\)](https://doi.org/10.1130/2011.2477(01))
- 779 Hiesinger, H., van der Bogert, C. H., Reiss, D., & Robinson, M. S. (2011b). Crater size-  
780 frequency distribution measurements of Mare Crisium. *42th Lunar and Planetary Science  
781 Conference*. Lunar and Planetary Institute, The Woodlands, Texas, abstract #2179.
- 782 Hurwitz, D. M., Head, J. W., Wilson, L., & Hiesinger, H. (2012). Origin of lunar sinuous rilles:  
783 Modeling effects of gravity, surface slope, and lava composition on erosion rates during the  
784 formation of Rima Prinz. *Journal of Geophysical Research: Planets*, 117(E12).  
785 <https://doi.org/10.1029/2011JE004000>
- 786 Hurwitz, D. M., Head, J. W., & Hiesinger, H. (2013). Lunar sinuous rilles: Distribution,  
787 characteristics, and implications for their origin. *Planetary and Space Science*, 79-80, 1-38.  
788 <https://doi.org/10.1016/j.pss.2012.10.019>
- 789 Ivanov, M. A., Head, J. W., & Bystrov, A. (2016). The lunar Gruithuisen silicic extrusive domes:  
790 Topographic configuration, morphology, ages, and internal structure. *Icarus*, 273, 262-283.  
791 <https://doi.org/10.1016/j.icarus.2015.12.015>
- 792 Jolliff, B. L., Gillis, J. J., Haskin, L. A., Korotev, R. L., & Wieczorek, M. A. (2000). Major lunar  
793 crustal terranes: Surface expressions and crust-mantle origins. *Journal of Geophysical  
794 Research: Planets*, 105(E2), 4197-4216. <https://doi.org/10.1029/1999JE001103>
- 795 Lawrence, D. J., Elphic, R. C., Feldman, W. C., Prettyman, T. H., Gasnault, O., & Maurice, S.  
796 (2003). Small-area thorium features on the lunar surface. *Journal of Geophysical Research:  
797 Planets*, 108(E9). <https://doi.org/10.1029/2003JE002050>
- 798 Lemelin, M., Lucey, P. G., Song, E., & Taylor, G. J. (2015). Lunar central peak mineralogy and  
799 iron content using the Kaguya Multiband Imager: Reassessment of the compositional structure  
800 of the lunar crust. *Journal of Geophysical Research: Planets*, 120(5), 869-887.  
801 <https://doi.org/10.1002/2014je004778>
- 802 Masursky, H., Colton, G. W., & El - Baz, F. (1978). *Apollo over the Moon: A view from orbit*  
803 (NASA SP-362), Washington, DC: Scientific and Technical Information Office.
- 804 Morota, T., Haruyama, J., Honda, C., Ohtake, M., Yokota, Y., Kimura, J., et al. (2009). Mare  
805 volcanism in the lunar farside Moscoviense region: Implication for lateral variation in magma  
806 production of the Moon. *Geophysical Research Letters*, 36(21).  
807 <https://doi.org/10.1029/2009GL040472>
- 808 Morota, T., Haruyama, J., Ohtake, M., Matsunaga, T., Honda, C., Yokota, Y., et al. (2011).  
809 Timing and characteristics of the latest mare eruption on the Moon. *Earth and Planetary  
810 Science Letters*, 302(3-4), 255-266. <https://doi.org/10.1016/j.epsl.2010.12.028>
- 811 Neish, C. D., Hamilton, C. W., Hughes, S. S., Nawotniak, S. K., Garry, W. B., Skok, J. R., et al.  
812 (2017). Terrestrial analogues for lunar impact melt flows. *Icarus*, 281, 73-89.  
813 <https://doi.org/10.1016/j.icarus.2016.08.008>
- 814 Nelson, D. M., Koeber, S. D., Daud, K., Robinson, M. S., Watters, T. R., Banks, M. E., &  
815 Williams, N. R. (2014). Mapping lunar maria extents and lobate scarps using LROC image  
816 products. *45th Lunar and Planetary Science Conference*. Lunar and Planetary Institute, The  
817 Woodlands, Texas, abstract #2961.
- 818 Pasckert, J. H., Hiesinger, H., & van der Bogert, C. H. (2015). Small-scale lunar farside  
819 volcanism. *Icarus*, 257, 336-354. <http://dx.doi.org/10.1016/j.icarus.2015.04.040>

- 820 Pasckert, J. H., Hiesinger, H., & van der Bogert, C. H. (2018). Lunar farside volcanism in and  
821 around the South Pole–Aitken basin. *Icarus*, 299(Supplement C), 538-562.  
822 <https://doi.org/10.1016/j.icarus.2017.07.023>
- 823 Qiao, L., Head, J., Wilson, L., Xiao, L., Kreslavsky, M., & Dufek, J. (2017). Ina pit crater on the  
824 Moon: Extrusion of waning-stage lava lake magmatic foam results in extremely young crater  
825 retention ages. *Geology*, 45(5), 455-458. <https://doi.org/10.1130/G38594.1>
- 826 Qiao, L., Head, J. W., Xiao, L., Wilson, L., & Dufek, J. D. (2018a). The role of substrate  
827 characteristics in producing anomalously young crater retention ages in volcanic deposits on  
828 the Moon: Morphology, topography, sub-resolution roughness and mode of emplacement of  
829 the Sosigenes Lunar Irregular Mare Patch (IMP). *Meteoritics & Planetary Science*, 53(4), 778-  
830 812. <https://doi.org/10.1111/maps.13003>.
- 831 Qiao, L., Head, J. W., Wilson, L., & Ling, Z. (2018b). Lunar irregular mare patch (IMP) sub-  
832 types: Linking their origin through hybrid relationships displayed at Cauchy 5 small shield  
833 volcano. *49th Lunar and Planetary Science Conference*. Lunar and Planetary Institute, The  
834 Woodlands, Texas, abstract #1392.
- 835 Qiao, L., Head, J. W., Ling, Z., Wilson, L., Xiao, L., Dufek, J. D., & Yan, J. (2019a). Geological  
836 characterization of the Ina shield volcano summit pit crater on the Moon: Evidence for  
837 extrusion of waning-stage lava lake magmatic foams and anomalously young crater retention  
838 ages. *Journal of Geophysical Research: Planets*, 124(4), 1100-1140.  
839 <https://doi.org/10.1029/2018JE005841>
- 840 Qiao, L., Head, J. W., Ling, Z., & Wilson, L. (2019b). Exploring a sub-classification scheme for  
841 Irregular Mare Patches (IMPs), *50th Lunar and Planetary Science Conference*, Lunar and  
842 Planetary Institute, The Woodlands, Texas, abstract #2358.
- 843 Qiao, L., Head, J. W., Wilson, L., & Ling, Z. (2020). The Cauchy 5 small, low-volume lunar  
844 shield volcano: Evidence for volatile exsolution-eruption patterns and type 1/type 2 hybrid  
845 irregular mare patch (IMP) formation. *Journal of Geophysical Research: Planets*, 125,  
846 e2019JE006171. <https://doi.org/10.1029/2019JE006171>
- 847 Robinson, M. S., Brylow, S. M., Tschimmel, M., Humm, D., Lawrence, S. J., Thomas, P. C., et  
848 al. (2010). Lunar Reconnaissance Orbiter Camera (LROC) instrument overview. *Space*  
849 *Science Reviews*, 150(1-4), 81-124. <https://doi.org/10.1007/s11214-010-9634-2>
- 850 Schultz, P. H. (1976). *Moon morphology*, Austin: University of Texas Press.
- 851 Schultz, P. H. (1991). The Moon: dead or alive. *Workshop on Mare Volcanism and Basalt*  
852 *Petrogenesis: "Astounding Fundamental Concepts (AFC)" Developed Over the Last Fifteen*  
853 *Years*. Lunar and Planetary Institute and Lunar and Planetary Sample Team (LAPST), Dallas,  
854 Texas, pp. 45-46.
- 855 Schultz, P. H., Staid, M. I., & Pieters, C. M. (2006). Lunar activity from recent gas release.  
856 *Nature*, 444(7116), 184-186. <https://doi.org/10.1038/nature05303>
- 857 Sim, C. K., Kim, S. S., Jeong, M., Choi, Y.-J., & Shkuratov, Y. G. (2019). Observational  
858 strategy for KPLO/PolCam measurements of the lunar surface from orbit. *Publications of the*  
859 *Astronomical Society of the Pacific*, 132(1007), 015004. [http://dx.doi.org/10.1088/1538-](http://dx.doi.org/10.1088/1538-3873/ab523d)  
860 [3873/ab523d](http://dx.doi.org/10.1088/1538-3873/ab523d)
- 861 Stooke, P. J. (2012). Lunar meniscus hollows. *43rd Lunar and Planetary Science Conference*,  
862 Lunar and Planetary Institute, The Woodlands, Texas, abstract #1011.
- 863 Stopar, J. D., Lawrence, S. J., Graham, L., Hamilton, J., Denevi, B., John, K. K., et al. (2019).  
864 Ina, Moon: Geologic setting, scientific rationale, and site characterization for a small planetary

- 865 lander concept. *Planetary and Space Science*, 171, 1-16.  
866 <https://doi.org/10.1016/j.pss.2019.04.003>
- 867 Strain, P. L., & El-Baz, F. (1980). The geology and morphology of Ina. In *Proceedings of the*  
868 *11th Lunar Science Conference* (pp. 2437-2446).
- 869 Tye, A. R., & Head, J. W. (2013). Mare Tranquillitatis: Distribution of mare domes, relation to  
870 broad mare rise, and evidence of a previously unrecognized basin from LOLA altimetric data.  
871 *44th Lunar and Planetary Science Conference*, Lunar and Planetary Institute, The Woodlands,  
872 Texas, abstract #1319.
- 873 Tyrle, A. (1988). Age dating of mare in the lunar crater Tsiolkovsky by crater-counting method.  
874 *Earth, Moon, and Planets*, 42(3), 245-264. <https://doi.org/10.1007/BF00058489>
- 875 Whitaker, E. A. (1972). An unusual mare feature, In *Apollo 15 Preliminary Science Report*  
876 (NASA SP-289, pp. 25-84–25-85).
- 877 Whitten, J., Head, J. W., Staid, M., Pieters, C. M., Mustard, J., Clark, R., et al. (2011). Lunar  
878 mare deposits associated with the Orientale impact basin: New insights into mineralogy,  
879 history, mode of emplacement, and relation to Orientale Basin evolution from Moon  
880 Mineralogy Mapper (M<sup>3</sup>) data from Chandrayaan-1. *Journal of Geophysical Research:*  
881 *Planets*, 116(E6). <https://doi.org/10.1029/2010JE003736>
- 882 Wilson, L., Hawke, B. R., Giguere, T. A., & Petrycki, E. R. (2011). An igneous origin for Rima  
883 Hyginus and Hyginus crater on the Moon. *Icarus*, 215(2), 584-595.  
884 <https://doi.org/10.1016/j.icarus.2011.07.003>
- 885 Wilson, L., & Head, J. W. (2017a). Generation, ascent and eruption of magma on the Moon:  
886 New insights into source depths, magma supply, intrusions and effusive/explosive eruptions  
887 (Part 1: Theory). *Icarus*, 283, 146-175. <https://doi.org/10.1016/j.icarus.2015.12.039>.
- 888 Wilson, L., & Head, J. W. (2017b). Eruption of magmatic foams on the Moon: Formation in the  
889 waning stages of dike emplacement events as an explanation of “irregular mare patches”.  
890 *Journal of Volcanology and Geothermal Research*, 335, 113-127.  
891 <https://doi.org/10.1016/j.jvolgeores.2017.02.009>
- 892 Wilson, L., & Head, J. W. (2018). Controls on lunar basaltic volcanic eruption structure and  
893 morphology: Gas release patterns in sequential eruption phases. *Geophysical Research Letters*,  
894 45(12), 5852-5859. <https://doi.org/10.1029/2018GL078327>
- 895 Yue, Z., Li, W., Di, K., Liu, Z., & Liu, J. (2015). Global mapping and analysis of lunar wrinkle  
896 ridges, *Journal of Geophysical Research: Planets*, 120, 978-994.  
897 <https://doi.org/10.1002/2014JE004777>
- 898 Zhang, F., Zhu, M. H., Bugiolacchi, R., Huang, Q., Osinski, G. R., Xiao, L., & Zou, Y. L.  
899 (2018). Diversity of basaltic lunar volcanism associated with buried impact structures:  
900 Implications for intrusive and extrusive events. *Icarus*, 307, 216-234.  
901 <https://doi.org/10.1016/j.icarus.2017.10.039>

902 **Tables**903 **Table 1.** Previous Theories for the Origin of Lunar IMPs and the Associated Deposits.

IMP origin theory	Reference	Interpretation of the associated deposits of lunar IMPs.
Sublimation*	Whitaker, 1972	Mounds: mare-like materials; floor terrain: potential sublimates.
Small lava intrusions within a collapse caldera atop an extrusive volcanic dome	El-Baz, 1972, 1973; Strain & El-Baz, 1980	Entire Ina structure: summit caldera; mounds: small lava intrusions (among the youngest volcanism on the Moon, but age not specifically determined).
Removal of surface regolith by episodic out-gassing within the past 10 Ma	Schultz et al., 2006	Exposure of long-buried ancient (>3.5 Ga) high-titanium mare basalts.
Lava flow inflation	Garry et al., 2012	Mounds: inflated lava flows; floor hummocky terrains: lava breakouts; blocky units: mass wasting exposures.
Small basaltic eruptions within the past 100 Ma	Braden, 2013; Braden et al., 2014	Mounds: small magma extrusions; floor units: disrupted lava pond crust.
Possible pyroclastic eruption (explains only Cauchy 5 IMP, not Ina)*	Carter et al., 2013	Pyroclastic deposits.
Lava lake processes and magmatic foam extrusion	Qiao et al., 2017, 2018a, 2019a; Wilson & Head, 2017b.	Floor hummocky and blocky units: solidified macrovesicular lava lake crust; mounds: solidified magmatic foams.

\*Symbol denotes relatively simplified origin theories that are deduced from general observations of one parameter.

905 **Table 2.** List of the 21 IMPs Additional to the Braden et al. (2014) Catalog.

Informal Name	Max. Length [m]	Lat [°]	Lon [°]	Host mare	Geologic context	IMP characteristics	Source reference
Al-Bakri-1	660	13.952	20.044	Tranquillitatis	mare plain	rough, bright and pitted surface within mare plain	Moon-Wiki site
Arago N	60	7.586	21.019	Tranquillitatis	mare plain; 1.3 km NE of #10 IMP in Braden et al. (2014) catalog	rough, bright and pitted surface within mare plain	Braden, 2013
Aratus D-2	100	24.757	7.995	Serenitatis	mare volcanic edifices	quasi-circular, rough and bright pits within mare plain	Masursky, 1978; also #14 in Stooke, 2012
Aratus D-3	70	24.726	8.069	Serenitatis	mare plain	quasi-circular, rough and bright pits within mare plain	Masursky, 1978; also #14 in Stooke, 2012
Aratus D-4	90	24.534	8.065	Serenitatis	mare plain	irregular rough and bright pits at the upper wall of a circular depression	Stooke, 2012, #16
Aratus D-5	150	24.497	8.130	Serenitatis	on the wall and rim of a linear rille	irregular and arched rough pits at the upper wall and rim of a circular depression	Stooke, 2012, #14
Aratus D-6	15	24.370	8.117	Serenitatis	mare plain	small, quasi-circular rough pits at the upper wall of a circular depression	Stooke, 2012, #15
Bessarion V-1	660	14.917	-33.7	Insularum	mare structures; in an area with a cluster of IMPs including #27, #51 and #64 IMPs in Braden et al. (2014) catalog	rough, bright pits with ridged, vermicular features on the floors	Stooke, 2012, #24
Bessarion V-2	150	14.839	-33.876	Insularum	mare structures; in an area with a cluster of IMPs including #27, #51 and #64 IMPs in Braden et al. (2014) catalog	rough, bright pits at the upper wall and rim of a circular depression	Stooke, 2012, #27
Bessarion V-3	200	14.55	-33.856	Insularum	slope of mare structures; in an area with a cluster of IMPs including #27, #51 and	rough, bright pits at slopes	Moon-Wiki site

Bessarion V-4	130	14.267	-33.566	Insularum	#64 IMPs in Braden et al. (2014) catalog mare plain; in an area with a cluster of IMPs including #27, #51 and #64 IMPs Braden et al. (2014) catalog	rough, bright pits at the upper wall of a circular depression	Moon-Wiki site
Boda E-1	50	13.089	-3.760	Sinus Aestuum	mare plain; 5 km north of #50 IMP in Braden catalog	irregular rough and bright pits at the upper wall of a circular depression	Stooke, 2012, #11
Brayley D	30	19.145	-32.579	Imbrium	on the rim of a quasi-elliptic vent	elliptic, rough and bright pit on the rim of a vent	Stooke, 2012, #13
Maclear-4	320	10.597	20.944	Tranquillitatis	mare plain; between #17 and #31 IMPs in Braden et al. (2014) catalog	arc-shaped, rough, bright pit within mare plain	Moon-Wiki site
Maclear-5	120	10.603	20.9	Tranquillitatis	mare plain; between #17 and #31 IMPs in Braden et al. (2014) catalog	elongated, rough, bright pit within mare plain	Moon-Wiki site
Maclear-6	500	9.283	20.766	Tranquillitatis	small shield volcano flank; 1.7 km NW of the Arago-5 IMP in the Braden et al. (2014) catalog	rough, and pitted surface	Moon-Wiki site
Secchi X-1	80	-0.289	42.800	Fecunditatis	mare plain	elongated, rough and bright pits at the wall of a very shallow depression	Stooke, 2012, #18
Secchi X-3	20	-0.339	42.804	Fecunditatis	mare plain	irregular, rough and bright pits at the wall of a very shallow depression	Stooke, 2012, #19
Secchi X-4	90	-1.883	43.176	Fecunditatis	mare plain; 6 km NW of #28 IMP in Braden et al. (2014) catalog	irregular, rough and bright pit	Zhang et al., 2018
Secchi X-5	25	-2.058	43.525	Fecunditatis	mare plain; 1.5 km north of #62 IMP in Braden et al. (2014) catalog	irregular rough and bright pits at the upper wall of a circular depression	Stooke, 2012, #21
Vera	70	26.342	-43.76	Oceanus Procellarum	volcanic vent floor	elongated, rough and bright pit	Zhang et al., 2018

906 **Table 3.** List of 91 IMPs and Their Characteristics and Classifications.

# <sup>1</sup>	Name	Max. Length [m]	Lat [°]	Lon [°]	Context class <sup>2</sup>	Characteristics class <sup>3</sup>	Floor terrain texture <sup>4</sup>	Host mare	Host mare age [Ga]	Citation <sup>5</sup>
1	Sosigenes	5000	8.335	19.071	3	1	1234567	Tranquillitatis	3.68	B14
2	Ina	3000	18.65	5.3	1	1	1234567	Lacus Felicitatis	3.54	B14
3	Cauchy-5	3000	7.169	37.592	12	1+2A+2B	1278	Tranquillitatis	3.62	B14
4	Maskelyne	3000	4.33	33.75	1	1+2A+2B	23478	Tranquillitatis	3.62	B14
5	Nubium	2000	-25.72	-27.681	34	1+2A+2B	2378	Nubium	3.63	B14
6	Ross-E-1	1200	10.46	23.547	5B	2A	2378	Tranquillitatis	3.68	B14
7	Maclear-2	800	9.102	20.298	5A	2A	2347	Tranquillitatis	3.68	B14
8	Aristarchus North	800	25.044	-46.767	5B	2A+2B	23467	Oceanus Procellarum	1.2	B14
9	Arago-5	750	9.23	20.824	2	2A	134	Tranquillitatis	3.68	B14
10	Unnamed	670	7.559	20.984	5B	2A	237	Tranquillitatis	3.68	B14
11	Jansen-1	600	11.669	32.659	5A	2A+2B	237	Tranquillitatis	3.57	B14
12	Unnamed	560	8.298	21.6	5A	2A+2B	237	Tranquillitatis	3.68	B14
13	Unnamed	550	9.58	25.514	5A	2A	237	Tranquillitatis	3.68	B14
14	Unnamed	500	7.348	20.897	5A	2A	1237	Tranquillitatis	3.68	B14
15	Maclear-1	430	8.891	21.487	5A	2A	237	Tranquillitatis	3.68	B14
16	Unnamed	400	9.112	21.758	5A	2A	278	Tranquillitatis	3.68	B14
17	Unnamed	400	10.31	21.36	5A	2A	237	Tranquillitatis	3.68	B14
18	Unnamed	350	8.67	17.51	5A	2A	123467	Tranquillitatis	3.68	B14
19	Unnamed	350	9.564	25.392	5A	2A	237	Tranquillitatis	3.68	B14
20	Unnamed	350	9.432	26.287	1	2B	234	Tranquillitatis	3.68	B14
21	Unnamed	350	21.653	-0.865	4	2A	2347	Imbrium	xx	B14
22	Unnamed	340	9.54	20.22	5A	2A	237	Tranquillitatis	3.68	B14
23	GEM30	330	37.919	-45.221	5B	2A	237	Unnamed	xx	B14
24	Unnamed	315	7.887	21.937	5A	2A	237	Tranquillitatis	3.68	B14
25	Jansen-2	300	11.235	32.806	5A	2A+2B	237	Tranquillitatis	3.57	B14
26	Unnamed	300	10.163	19.228	5A	2A	237	Tranquillitatis	3.68	B14
27	Unnamed	300	14.44	-33.656	5B	2B	89	Insularum	2.12	B14
28	GEM1	300	38.152	-44.6	5B	2A	237	Unnamed	xx	B14
29	Unnamed	280	10.045	25.247	5A	2A+2B	378	Tranquillitatis	3.68	B14
30	Manilus-1	270	14.889	6.467	3	2A	2378	Vaporum	3.23	B14

31	Unnamed	270	10.77	20.52	5A	2A	278	Tranquillitatis	3.68	B14
32	Unnamed	255	9.102	20.265	5A	2A	237	Tranquillitatis	3.68	B14
33	Unnamed	250	9.894	24.851	5B	2A	237	Tranquillitatis	3.68	B14
34	Unnamed	250	37.121	-40.626	5A	2A	378	Imbrium	xx	B14
35	Unnamed	230	8.279	9.319	5B	2A+2B	237	Vaporum	3.73	B14
36	Carrel-1	200	9.817	25.519	5A	2A+2B	2378	Tranquillitatis	3.68	B14
37	Manilus-2	200	14.628	6.821	1	2B	8	Vaporum	3.23	B14
38	Unnamed	200	9.244	23.924	5A	2A	2378	Tranquillitatis	3.68	B14
39	GEM24	200	37.428	-43.543	5A	2A	78	Unnamed	xx	B14
40	GEM4	190	38.09	-44.584	5B	2A	378	Unnamed	xx	B14
41	GEM28	175	37.304	-43.628	5A	2B	278	Unnamed	xx	B14
42	Unnamed	170	4.096	21.218	5A	2A	378	Tranquillitatis	3.71	B14
43	GEM3	170	38.115	-44.677	5B	2A	23478	Unnamed	xx	B14
44	Unnamed	160	8.844	21.762	5A	2A+2B	2378	Tranquillitatis	3.68	B14
45	Unnamed	160	13.131	-4.361	4	2B	2378	Sinus Aestuum	xx	B14
46	Hyginus	150	7.726	6.35	3	2A+2B	2378	Vaporum	3.73	B14
47	Unnamed	150	7.083	38.574	5A	2A	378	Tranquillitatis	3.62	B14
48	Unnamed	150	8.714	19.383	5A	2B	28	Tranquillitatis	3.68	B14
49	Unnamed	150	10.101	25.278	5A	2A	378	Tranquillitatis	3.68	B14
50	Unnamed	150	12.931	-3.806	4	2B	189	Sinus Aestuum	xx	B14
51	Unnamed	150	14.597	-33.979	5B	2A+2B	78	Insularum	2.12	B14
52	GEM21	150	37.882	-44.288	5B	2B	2789	Unnamed	xx	B14
53	GEM32	140	37.826	-45.129	5B	2A	237	Unnamed	xx	B14
54	GEM7	140	38.058	-44.073	5A	2B	78	Unnamed	xx	B14
55	Unnamed	130	4.55	22.882	5A	2A+2B	2478	Tranquillitatis	3.58	B14
56	Unnamed	130	2.934	38.975	5A	2A+2B	78	Tranquillitatis	3.5	B14
57	GEM11	130	37.941	-44.218	5B	2B	89	Unnamed	xx	B14
58	Unnamed	125	-2.008	43.333	5A	2B	278	Fecunditatis	3.47	B14
59	GEM 31	120	38.018	-44.113	5A	2B	78	Unnamed	xx	B14
60	Unnamed	100	9.012	22.248	5B	2A	78	Tranquillitatis	3.68	B14
61	Unnamed	100	9.738	22.32	5B	2A	78	Tranquillitatis	3.68	B14
62	Unnamed	100	-2.113	43.512	5A	2B	78	Fecunditatis	3.47	B14

63	Unnamed	100	26.786	-42.959	4	2A+2B	34678	Oceanus Procellarum	3.48	B14
64	Unnamed	100	14.468	-33.729	5B	2A+2B	9	Insularum	2.12	B14
65	GEM35	100	36.937	-44.121	5B	2B	378	Unnamed	xx	B14
66	GEM29	100	37.904	-45.08	5B	2A	2378	Unnamed	xx	B14
67	GEM26	100	37.417	-43.577	5A	2A	78	Unnamed	xx	B14
68	GEM17	100	37.974	-44.285	5B	2B	78	Unnamed	xx	B14
69	GEM12	100	37.995	-44.159	5A	2B	78	Unnamed	xx	B14
70	GEM6	100	37.864	-44.478	5B	2A+2B	78	Unnamed	xx	B14
71	Al-Bakri-1	660	13.952	20.044	5A	2A+2B	237	Tranquillitatis	3.68	MW
72	Arago N	60	7.586	21.019	5B	2A+2B	78	Tranquillitatis	3.68	B13
73	Aratus D-2	100	24.757	7.995	5B	2A+2B	48	Serenitatis	3.3	M78, S12
74	Aratus D-3	70	24.726	8.069	5A	2A	478	Serenitatis	3.3	M78, S12
75	Aratus D-4	90	24.534	8.065	5A	2B	78	Serenitatis	3.3	S12
76	Aratus D-5	150	24.497	8.130	4	2A	78	Serenitatis	3.3	S12
77	Aratus D-6	15	24.370	8.117	5A	2B	78	Serenitatis	3.3	S12
78	Bessarion-V-1	660	14.92	-33.7	5B	2A+2B	247	Insularum	2.12	MW
79	Bessarion-V-2	150	14.84	-33.885	5B	2A+2B	78	Insularum	2.12	MW
80	Bessarion-V-3	200	15.56	-33.86	5B	2B	89	Insularum	2.12	MW
81	Bessarion-V-4	130	14.27	-33.57	5A	2B	78	Insularum	2.12	MW
82	Boda E-1	50	13.089	-3.760	5A	2B	78	Sinus Aestuum	xx	S12
83	Brayley D	30	19.145	-32.579	4	2A	78	Imbrium	2.12	S12
84	Maclear-4	320	10.6	20.94	5A	2A	278	Tranquillitatis	3.68	MW
85	Maclear-5	120	10.604	20.9	5A	2A	78	Tranquillitatis	3.68	MW
86	Maclear-6	500	9.283	20.766	2	2A	238	Tranquillitatis	3.68	MW
87	Secchi X-1	80	-0.289	42.800	5A	2B	78	Fecunditatis	3.53	S12
88	Secchi X-3	20	-0.339	42.804	5A	2B	78	Fecunditatis	3.53	S12
89	Secchi X-4	90	-1.882	43.176	5A	2A	7	Fecunditatis	3.47	S12
90	Secchi X-5	25	-2.058	43.525	5A	2B	78	Fecunditatis	3.47	S12
91	Vera	70	26.342	-43.76	3	2A	78	Oceanus Procellarum	3.48	Z18

<sup>1</sup>#1-70 IMPs are those listed in the Table S1 of Braden et al., (2014), others are additional IMPs in Table 2.

<sup>2</sup>Lunar IMP geologic context class: small shield volcano summit pit floor (Context #1) and flank (Context #2), pit crater chain or linear/sinuuous rille interior (Context #3) and adjacent exterior (Context #4) and typical mare deposits (Context #5A: mare plain and Context #5B: mare features and

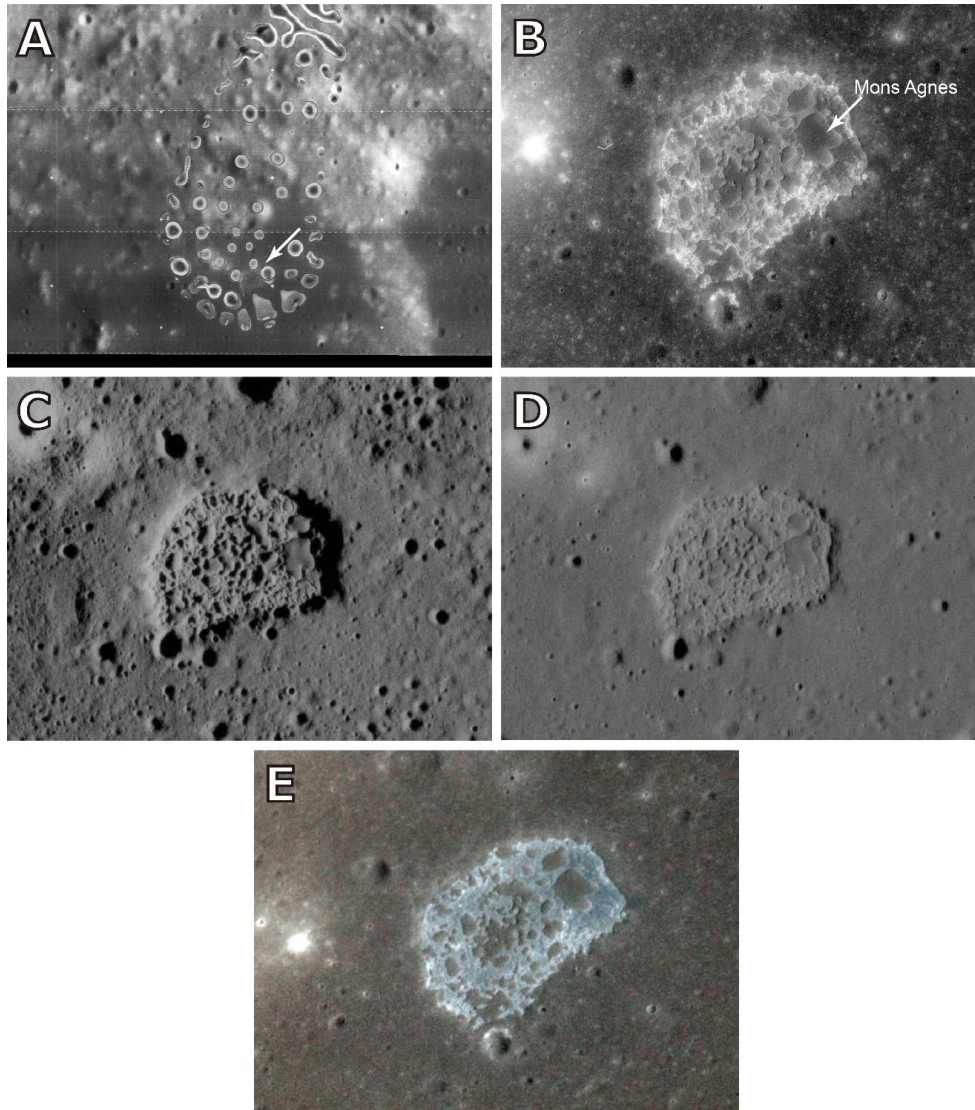
---

structures), a multiple-digital number indicates a combination of the multiple classes, e.g., “12” means this IMP contains both type #1 and #2 geologic settings (same for characteristics class and floor terrain texture encodings).

<sup>3</sup>Lunar IMP characteristic class: “mound + floor” type (Class #1) and “pit only” type (Class #2A: within maria and Class #2B: associated with depressions).

<sup>4</sup>Floor terrain texture types: 1) smooth terrain, 2) hummocky, 3) pitted, 4) ridged, 5) polygonal, 6) vermicular, 7) blocky, 8) uneven and 9) bright streak.

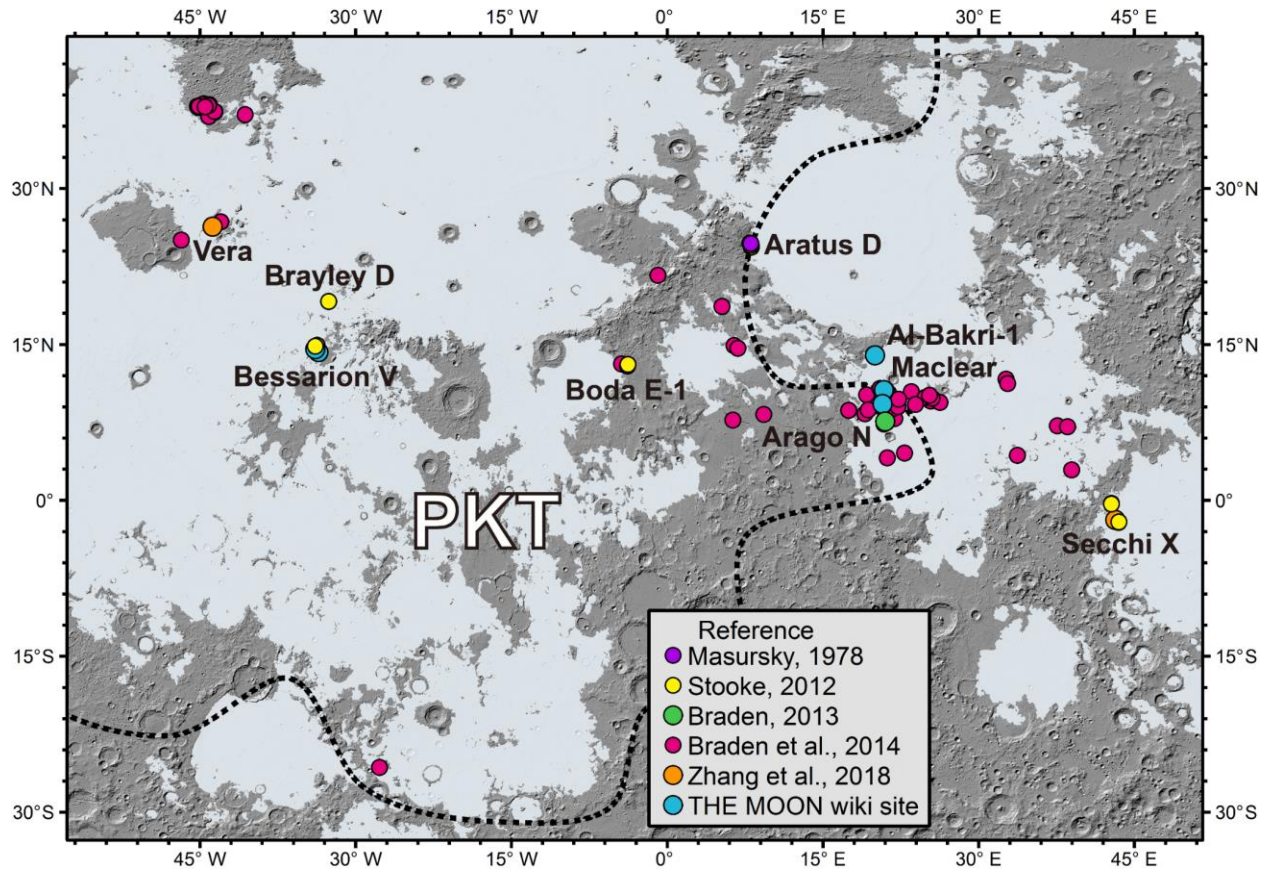
<sup>5</sup>Citation: source reference for IMP identifications, B13: Braden, 2013, B14: Braden et al., 2014, M78: Masursky, 1978, S12: Stooke, 2012, MW: THE MOON wiki site and Z18: Zhang et al., 2018. Note some identifications by Braden et al., (2014) have been previously reported (see their Table S1).

908 **Figures**

909

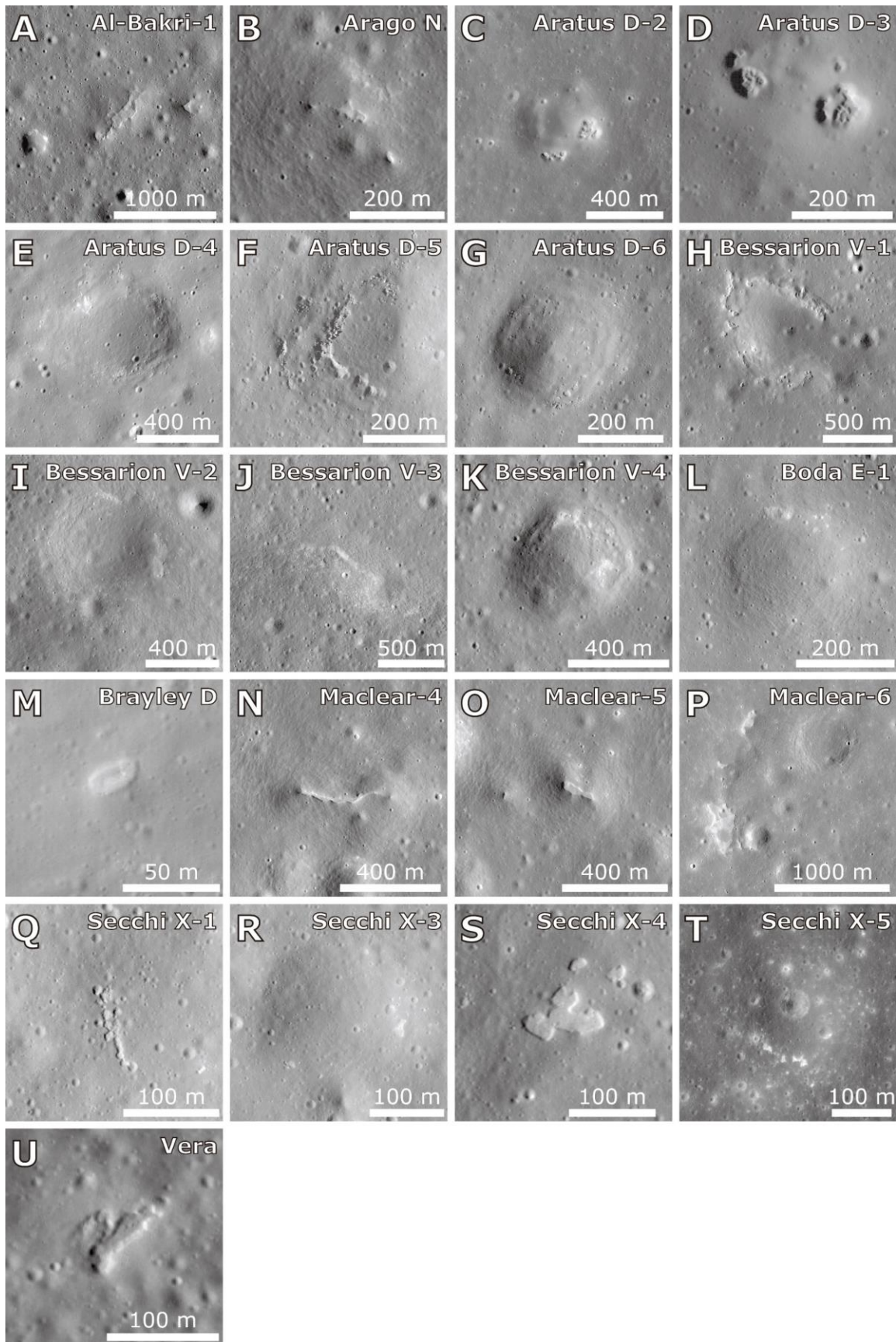
910 **Figure 1.** Views of the Ina feature obtained during the Apollo era: (A) Lunar Orbiter photograph,  
 911 portion of frame IV-102-H3, solar angle (from horizon)  $68.4^\circ$ , Ina feature is pointed out; (B)  
 912 Apollo 15 Panoramic Camera photo, portion of frame AS15-P-0181, solar angle  $65.0^\circ$ , Mons  
 913 Agnes is pointed out; (C) Apollo 17 Metric Camera photo, portion of frame AS17-M-1518, solar  
 914 angle  $4.0^\circ$ ; (D) Apollo 17 Metric Camera photo, portion of frame AS17-M-1821, solar angle  
 915  $13.0^\circ$ ; (E) Apollo 17 color Hasselblad Camera (70 mm) photograph, portion of frame AS17-152-  
 916 23287, solar angle  $46^\circ$ .

917

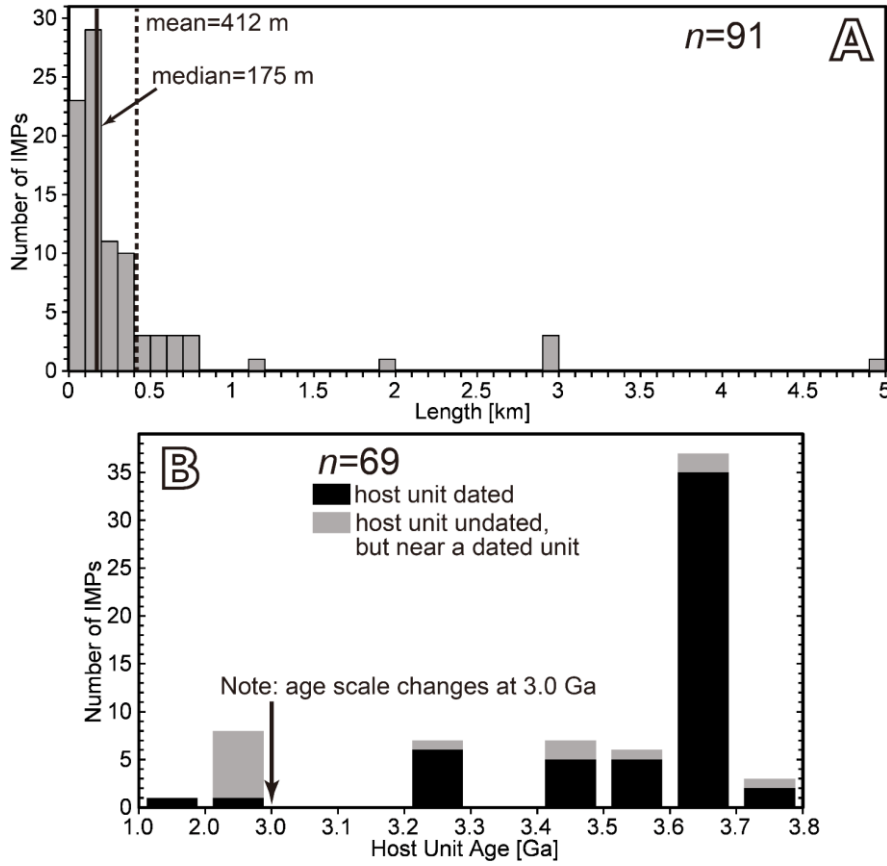


918

919 **Figure 2.** Spatial distribution map of the updated IMP population from several references (see  
 920 the legend in the lower left corner). The 21 IMPs additional to the Braden et al. (2014) catalog  
 921 are labelled (Table 2). Basemap is a hillshade (315° azimuth and 45° altitude) rendering of  
 922 LOLA 128 pixel/degree topography; exposed mare basalts mapped by Nelson et al. (2014) are  
 923 shown in white. The boundary of the Procellarum KREEP Terrane (PKT) is delineated by the  
 924 dashed white line, which is defined by the thorium 3.5 ppm contour line based on the criteria  
 925 established by Jolliff et al. (2000). The projection is simple cylindrical centered at 0°E, 0°N, and  
 926 north is up (the same in Figures 5, 6 and 13).

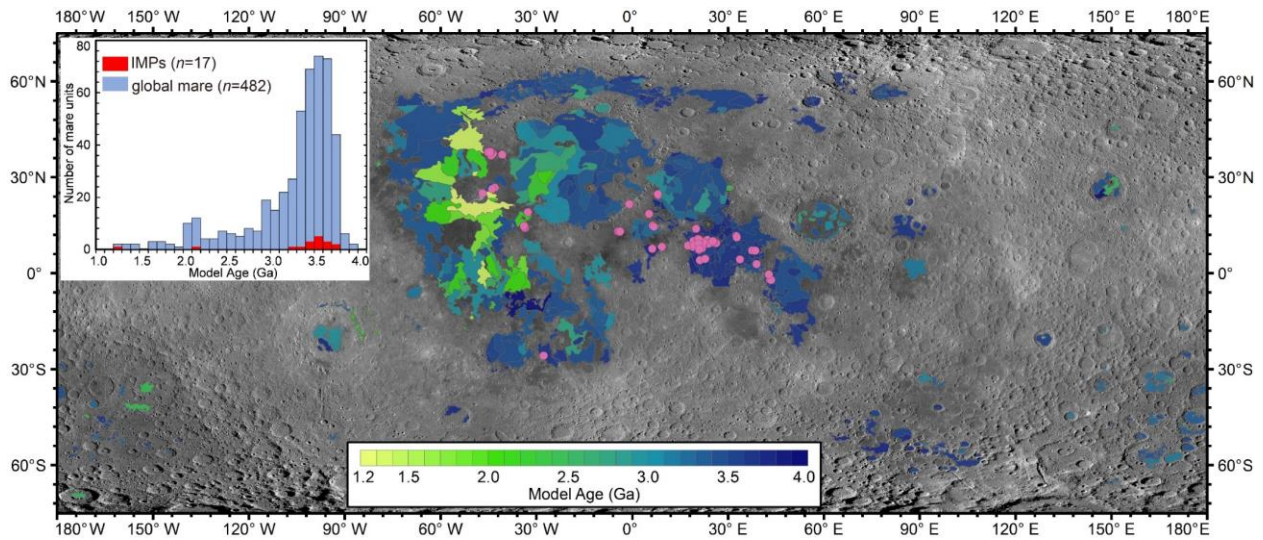


928 **Figure 3.** LROC NAC images of the 21 IMPs added to the Braden et al. (2014) catalog: (A) Al-  
929 Bakri-1 (the informal name corresponds to that in Table 2), NAC frame M1127000272R, 1.15  
930 m/pixel, 73.71° incidence angle ( $i$ ); (B) Arago N, LROC NAC frame M1096358215L, 1.16 m  
931 pixel size, 71.06° incidence angle; this IMP is ~1.3 km NE of the #10 IMP in the Braden et al.  
932 (2014) catalog; (C) Aratus D-2, NAC frame M104469044R, 1.45 m/pixel,  $i = 57.64^\circ$ ; (D) Aratus  
933 D-3, NAC frame M1218899889L, 1.03 m/pixel,  $i = 69.50^\circ$ ; (E) Aratus D-4, NAC frame  
934 M1200072847L, 1.11 m/pixel,  $i = 68.24^\circ$ ; (F) Aratus D-5, NAC frame M150464022L (also for  
935 panel G), 0.47 m/pixel,  $i = 64.01^\circ$ ; (G) Aratus D-6; (H) Bessarion V-1, NAC frame  
936 M1123818323L, 1.22 m/pixel,  $i = 71.34^\circ$ ; (I) Bessarion V-2, NAC frame M1123818323R (also  
937 for panel J), 1.22 m/pixel,  $i = 71.35^\circ$ ; (J) Bessarion V-3; (K) Bessarion V-4, NAC frame  
938 M1173279016L, 1.19 m/pixel, 70.16° incidence angle; the Bessarion V IMPs (#1-4), along with  
939 three IMPs identified in the Braden et al. (2014) catalog (#27, #51 and #64), occur in a ~20×13  
940 km area ~31 km west of the Bessarion V crater in northern margin of Mare Insularum; (L) Boda  
941 E-1, NAC frame M150545226L, 0.47 m/pixel,  $i = 61.73^\circ$ ; this IMP is 5 km north of #50 IMP in  
942 Braden et al. (2014) catalog; (M) Brayley D, NAC frame M144836594L, 0.50 m/pixel,  $i =$   
943  $53.81^\circ$ ; (N) Maclear-4, NAC frame M181030493L (also for panel O), 1.19 m/pixel,  $i = 67.74^\circ$ ;  
944 (O) Maclear-5; Maclear 4 and 5 IMPs are 1.1 km apart and they lie between the #17 and #31  
945 IMPs (28.7 km apart) in the Braden et al. (2014) catalog; (P) Maclear-6, NAC frame  
946 M1184689380R, 1.07 m m/pixel,  $i = 68.18^\circ$ ; this IMP is 1.7 km NW of the Arago-5 IMP in  
947 Braden et al. (2014) catalog, which are both on the flank of a small shield volcano; (Q) Secchi X-  
948 1, NAC frame M119571034R (also for panel R), 0.48 m/pixel,  $i = 57.24^\circ$ ; (R) Secchi X-3; (S)  
949 Secchi X-4, NAC frame M1249261996R, 0.84 m/pixel size,  $i = 65.63^\circ$ ; this IMP is 6 km NW of  
950 #28 IMP in Braden et al. (2014) catalog; (T) Secchi X-5, NAC frame M121925686R, 0.48  
951 m/pixel,  $i = 29.77^\circ$ ; this IMP is 1.5 km north of #62 IMP in Braden et al. (2014) catalog; (U)  
952 Vera, NAC frame M1173350317R, 1.27 m/pixel,  $i = 71.29^\circ$ . All panels are sinusoidally  
953 projected with map center at the IMP identification site, and north is up (the same in Figures 7-  
954 12, 14 and 15).



955

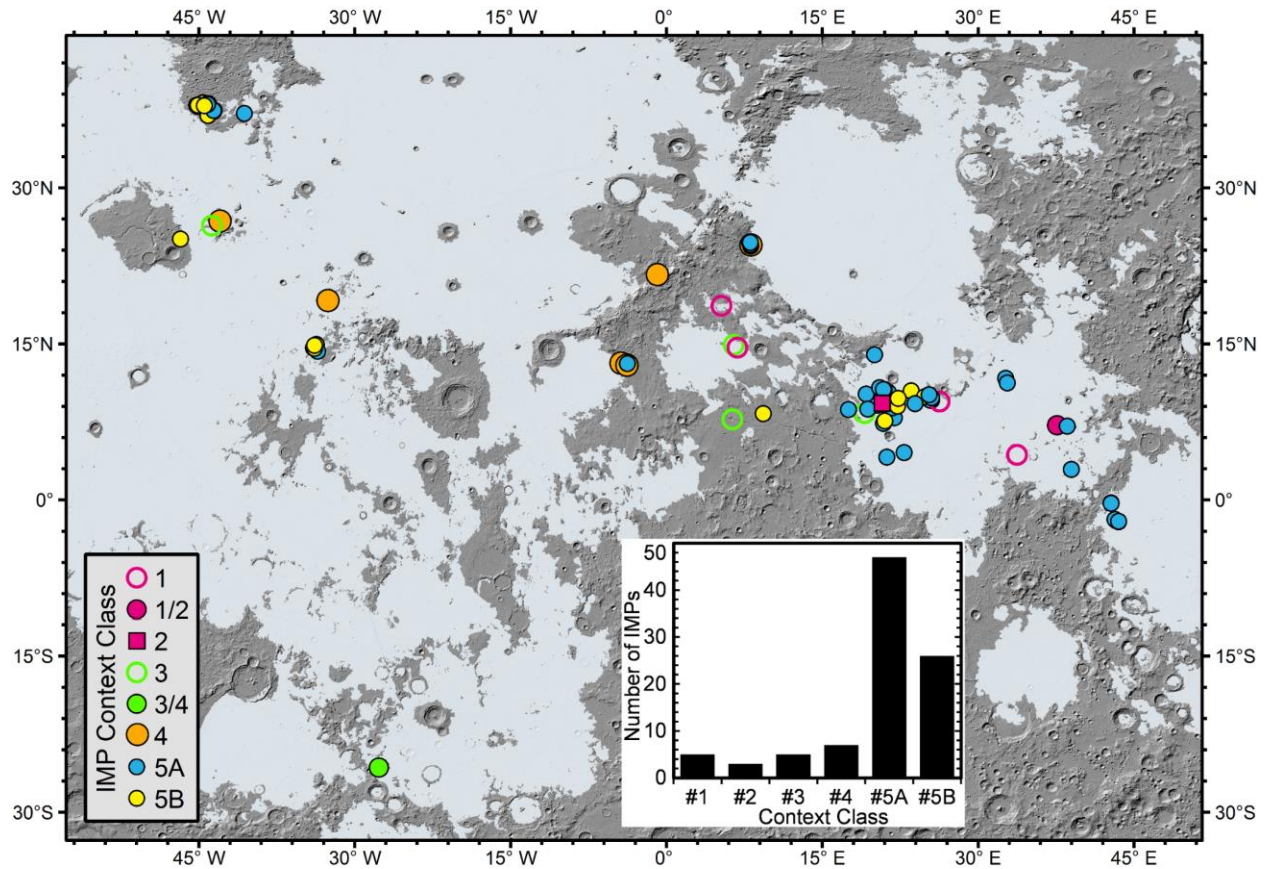
956 **Figure 4.** Histograms of (A) the maximum length of the 91 IMPs and (B) host mare unit age of  
 957 69 IMPs. The length-frequency of lunar IMPs (panel A) shows a leptokurtic distribution, with a  
 958 positive skewness toward larger sizes, mean length of 412 m and median length value of 175 m.  
 959 Note the horizontal axis (host mare age) scale of panel B changes at 3.0 Ga.



960

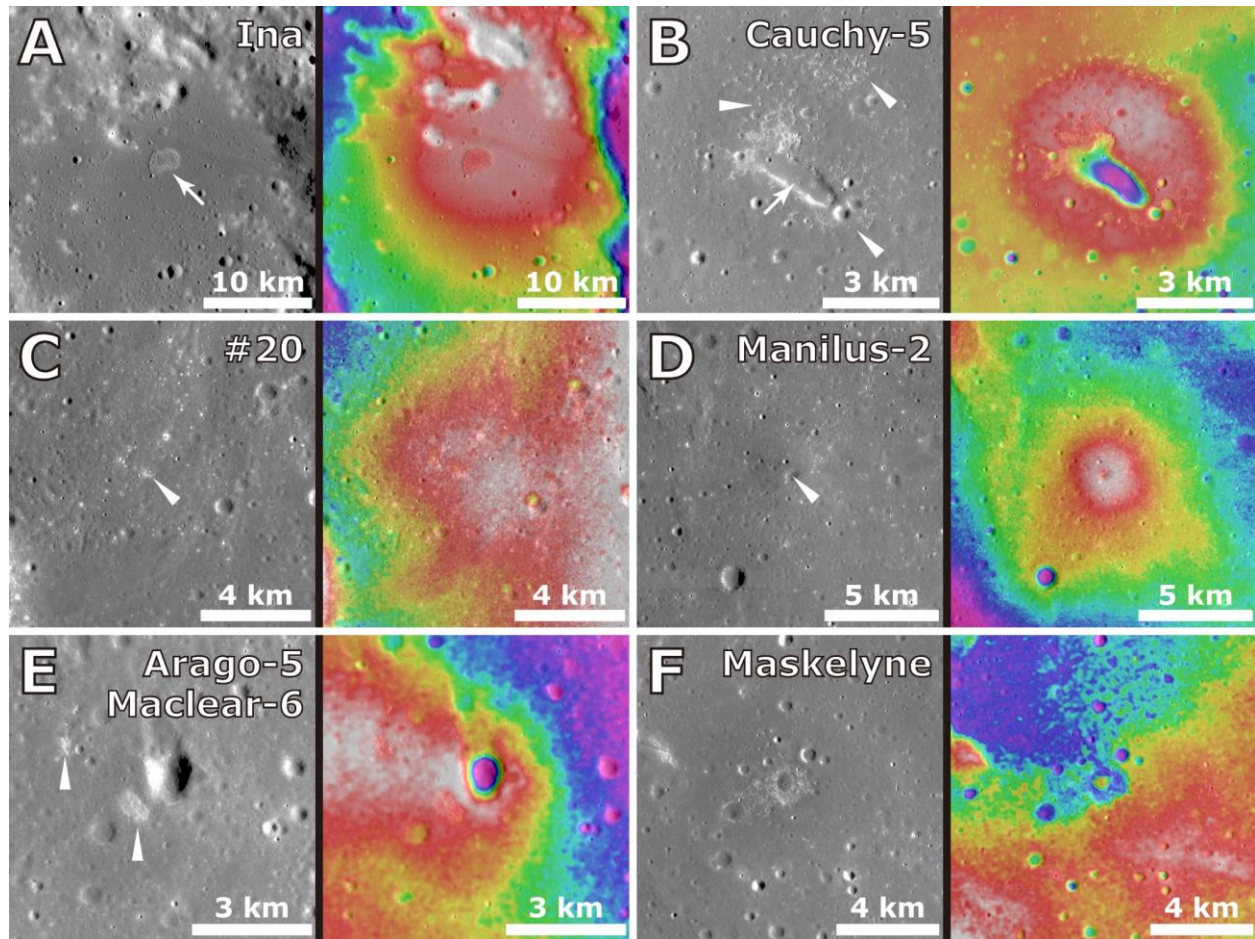
961 **Figure 5.** Distribution of the entire IMP population (pink dots) in the context of the global map  
 962 of the model ages of mare basalts (color-coded). The insert panel shows the histogram of the

963 temporal distribution of model ages of global lunar mare units (blue columns) and host mare unit  
 964 ages of lunar IMPs (red columns). The model ages of global mare units ( $n = 482$ ) are compiled  
 965 from multiple previous investigations (Cho et al., 2012; Haruyama et al., 2009; Hiesinger et al.,  
 966 2006, 2011a, 2011b; Morota et al., 2009, 2011; Pasckert et al., 2015, 2018; Tyrie, 1998; Whitten  
 967 et al., 2011).



968

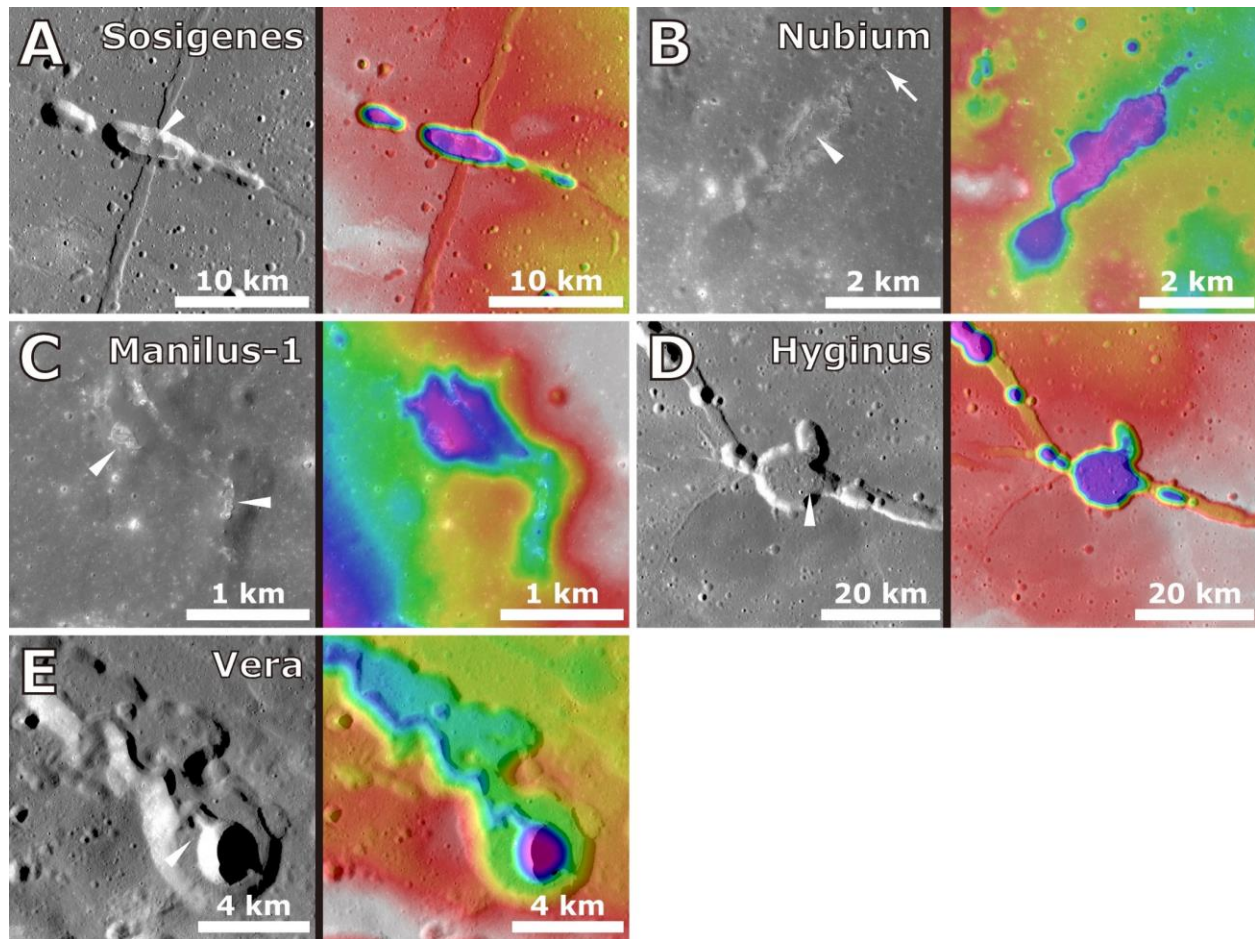
969 **Figure 6.** Spatial distribution of all identified IMPs in terms of the classification of their geologic  
 970 context. The insert panel shows the histogram of IMP population in each context type.



971

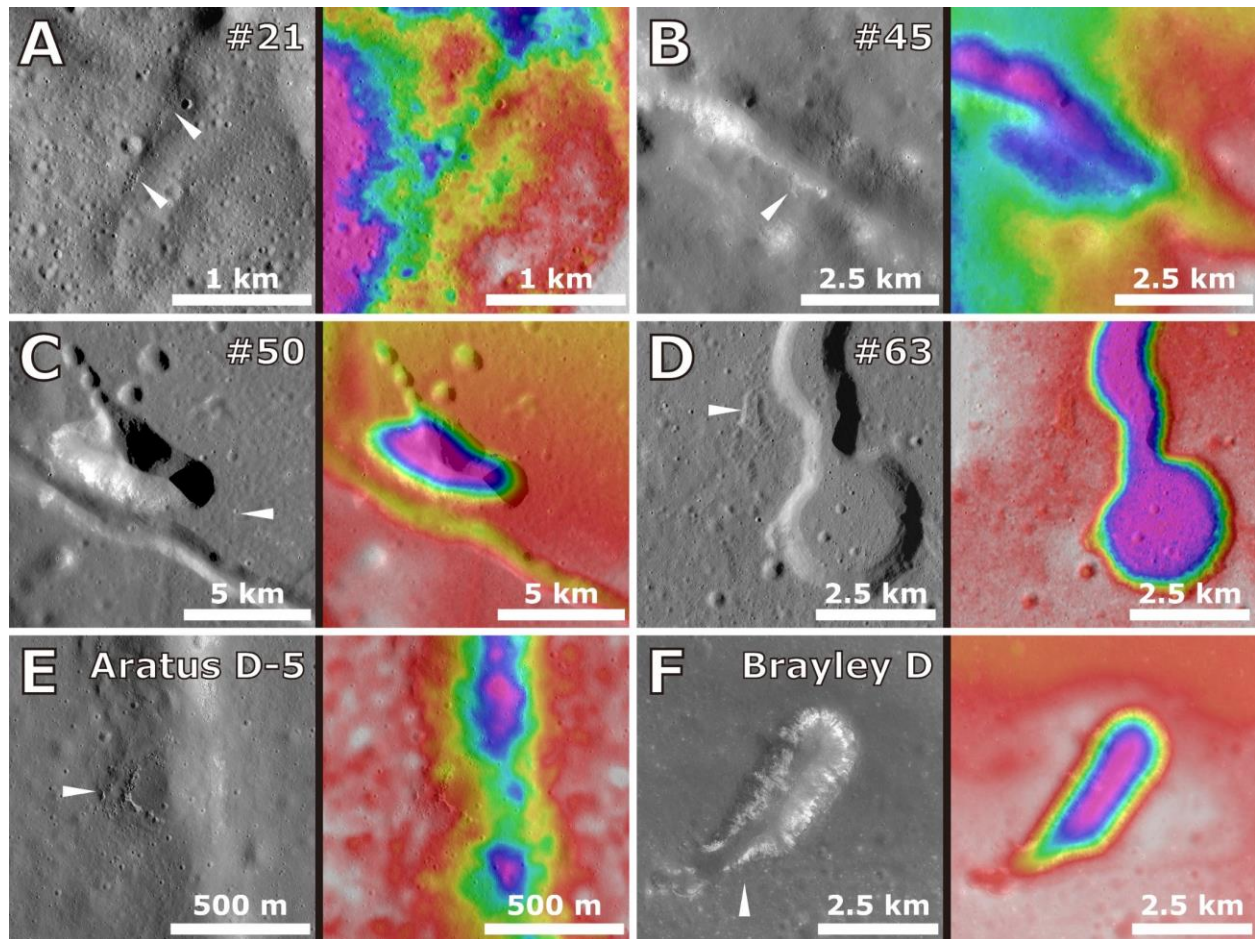
972 **Figure 7.** The geological context of lunar IMPs associated with small shield volcanos: on the  
 973 summit pit crater floor (Context #1; panels A-D) and on the flank (Context #2; panels B and E),  
 974 and one possible Context #1 IMP (panel F). Each site is shown in an optical image (left column)  
 975 and with a color topography map overlain (right column; red and white colors are higher  
 976 elevations and purple and magenta colors are lower elevations). (A) Ina, 18.65°N, 5.3°E, the  
 977 arrow points to the IMP feature on the small shield pit crater floor, Kaguya TC evening map and  
 978 SLDEM2015 topography. (B) Cauchy-5, 7.169°N, 37.592°E, the arrow points to the IMP  
 979 occurrence on the small shield pit crater floor (Context #1 IMP) and the tips of elongated triangle  
 980 mark the IMPs on the shield flank (Context #2 IMPs), LROC NAC M1108025067 and LROC  
 981 NAC DTM. (C) #20 IMP, 9.432°N, 26.287°E, the tip of elongated triangle marks the IMP on  
 982 shield summit pit crater floor, TC morning map and TC DTM topography. (D) Manilus-2,  
 983 14.628°N, 6.821°E, the tip of elongated triangle marks the IMP on shield summit pit crater floor,  
 984 TC morning map and TC DTM topography. (E) Arago-5 small shield, 9.259°N, 20.788°E, which  
 985 hosts two IMPs on its flank: Arago-5 IMP (marked by the lower right elongated triangle) and  
 986 Maclear-6 IMP (the upper left elongated triangle; Table 2), TC morning map and TC DTM  
 987 topography. (F) Maskelyne, 4.33°N, 33.75°E, TC morning map and TC DTM topography.

988



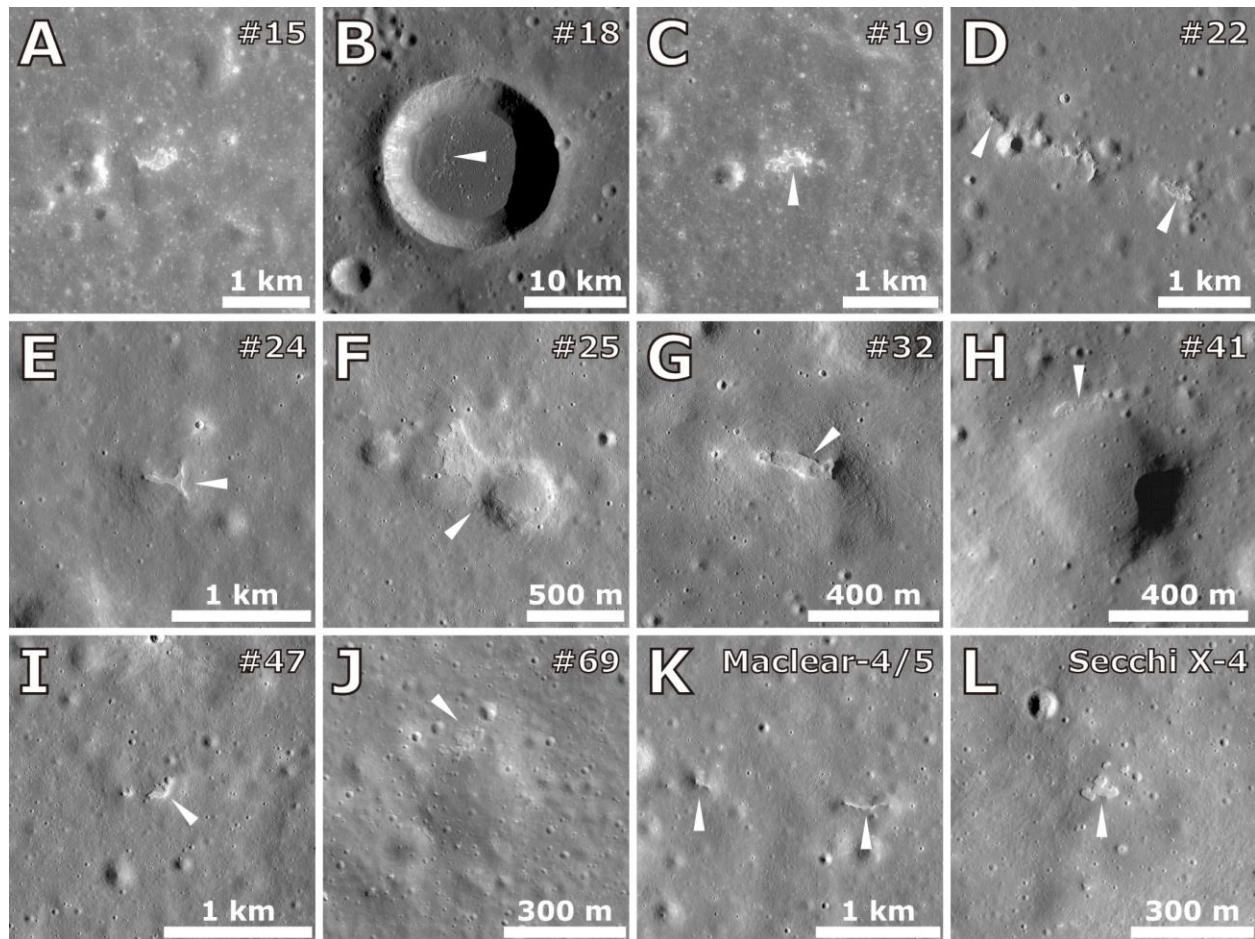
989

990 **Figure 8.** The geological context of lunar IMPs within linear/sinuuous rilles or pit crater chains  
 991 (Context #3 IMPs). Each site is shown in an optical image (left column) and with color  
 992 topography map overlain (right column; red and white colors are higher elevations and purple  
 993 and magenta colors are lower elevations). (A) Sosigenes, 8.335°N, 19.071°E, Kaguya TC  
 994 evening map and TC DTM topography. (B) Nubium, 25.724°S, 27.681°W, LROC NAC  
 995 M1167355858 and NAC DTM topography. (C) Manilus-1, 14.889°N, 6.467°E, NAC  
 996 M1121188383 and NAC DTM topography. (D) Hyginus, 7.726°N, 6.35°E, TC morning map and  
 997 TC DTM topography. (E) Vera, 26.342°N, 43.76°W, TC morning map and TC DTM topography.  
 998 IMPs in pits are all marked by white elongated triangles and the arrow in panel B points to an  
 999 IMP occurrence outside the pit crater (a Context #4 IMP).



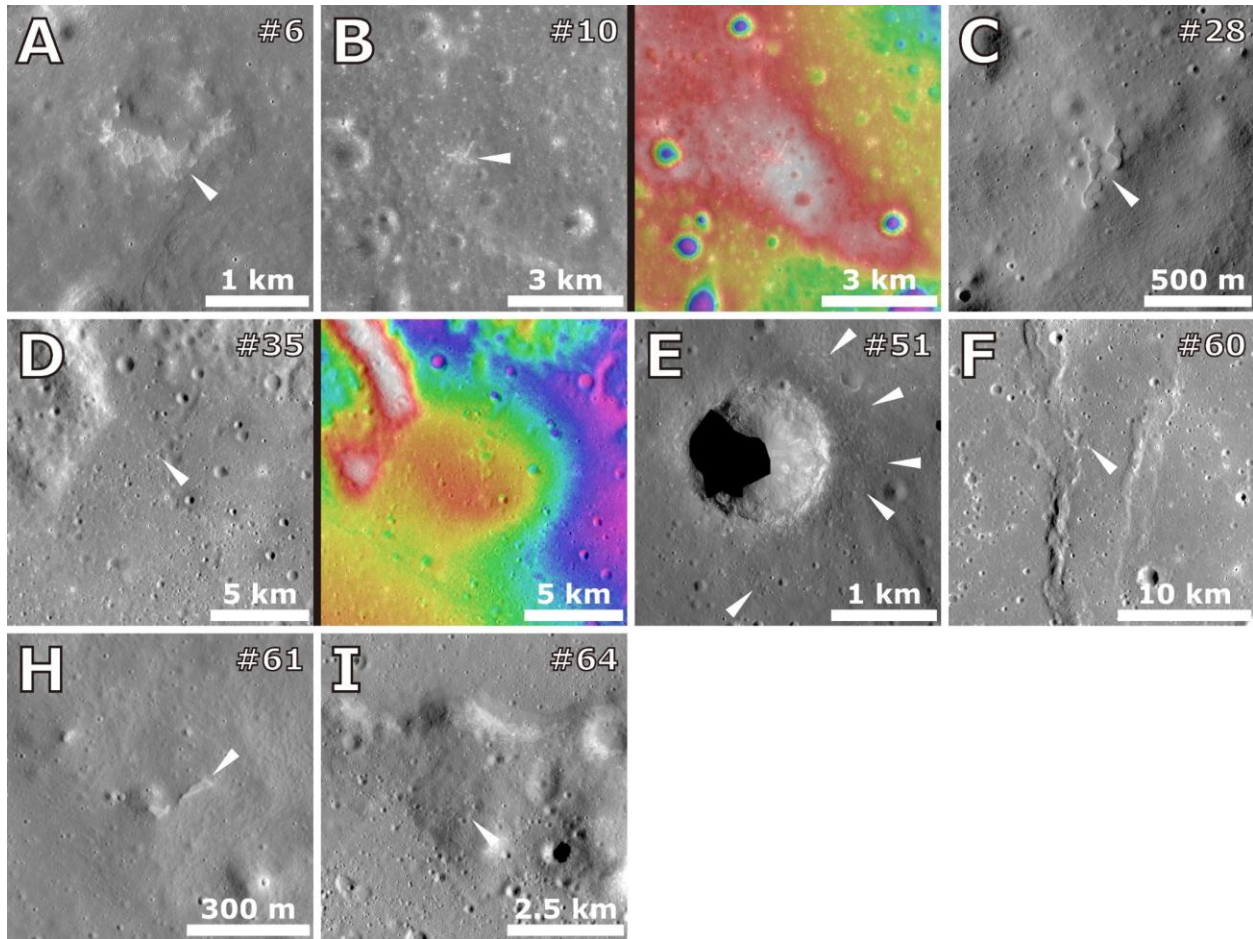
1000

1001 **Figure 9.** The geological context of lunar IMPs on the rim (panels A, B, E and F) or in the  
 1002 adjacent exterior (panels C and D) of linear/sinuuous rilles (Context #4 IMPs). Each site is shown  
 1003 in an optical image (left column) and with a color topography map overlain (right column; red  
 1004 and white colors are higher elevations and purple and magenta colors are lower elevations). (A)  
 1005 #21 IMP (in the Braden et al. (2014) catalog), 21.653°N, 0.865°W, LROC NAC M1203670820R  
 1006 and TC DTM topography (the rille is too small to be well resolved on the 10 m/pixel TC  
 1007 topography). (B) #45 IMP, 13.131°N, 4.361°W, NAC M1138937683L and TC DTM topography.  
 1008 (C) #50 IMP, 12.931°N, 3.806°W, TC morning map and TC DTM topography. (D) #63 IMP,  
 1009 26.786°N, 42.959°W, NAC M1123882552L and TC DTM topography. (E) Aratus D-5 IMP  
 1010 (Table 2), 24.497°N, 8.130°E, NAC M150464022L and TC DTM topography. (F) Brayley D  
 1011 IMP (Table 2), 19.145°N, 32.579°W, NAC M1190926639 and NAC DTM topography. The  
 1012 IMPs are all marked by white elongated triangles.



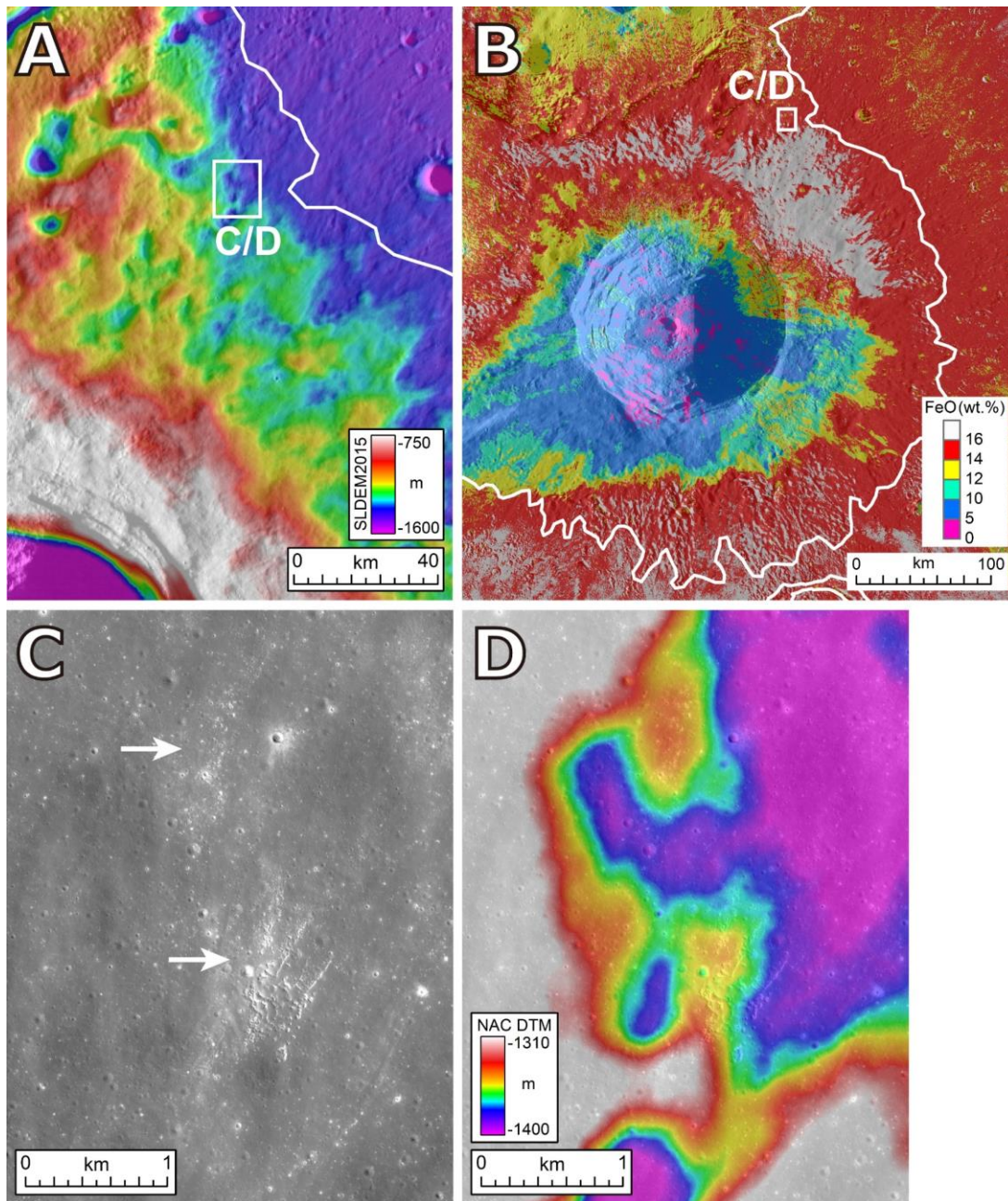
1013

1014 **Figure 10.** The geological context of representative IMPs in flat mare plains (Context #5A  
 1015 IMPs). (A) #15 IMP (in the Braden et al. (2014) catalog), 8.891°N, 21.487°E, LROC NAC  
 1016 M1175268761. (B) #18 IMP, 8.67°N, 17.51°E, Kaguya TC morning map. (C) #19 IMP, 9.564°N,  
 1017 25.392°E, NAC M1190554377. (D) #22 IMP, 9.54°N, 20.22°E, NAC M162175239. (E) #24  
 1018 IMP, 7.887°N, 21.937°E, NAC M181023296L. (F) #25 IMP, 11.235°N, 32.806°E, NAC  
 1019 M1157535724. (G) #32 IMP, 9.102°N, 20.265°E, NAC M162175239L. (H) #41 IMP, 37.304°N,  
 1020 43.628°W, NAC M1154514667L. (I) #47 IMP, 7.083°N, 38.574°E, NAC M180916096R. (J)  
 1021 #69 IMP, 37.995°N, 44.159°W, NAC M1280383538R. (K) Maclear-4 IMP (left), 10.6°N,  
 1022 20.94°E and Maclear-5 IMP (right), 10.604°N, 20.9°E, NAC M181030493L. (L) Secchi X-4  
 1023 IMP, 1.882°S, 43.176°E, NAC M1249261996R. The IMPs are all marked by the white elongated  
 1024 triangles.



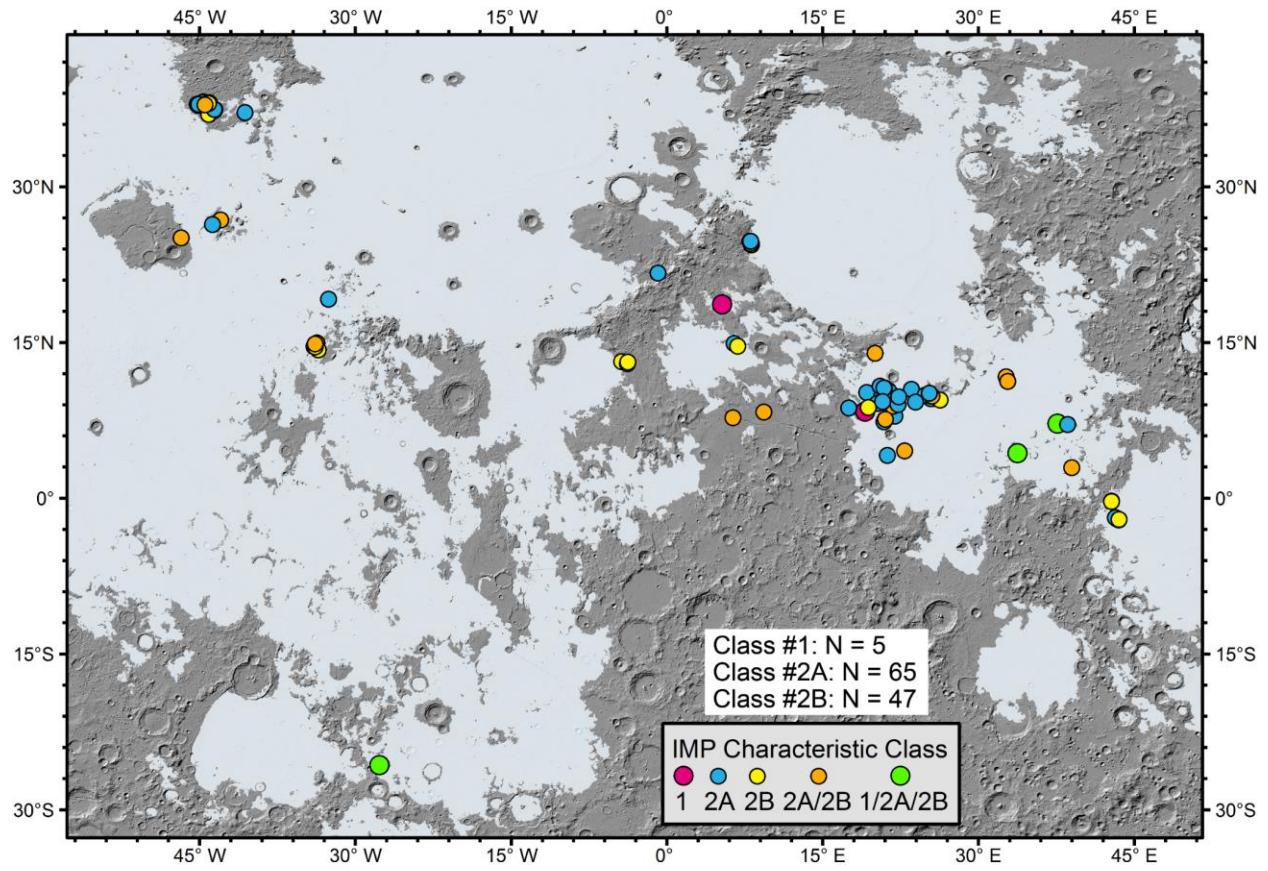
1025

1026 **Figure 11.** The geological context of representative IMPs in mare features and structures  
 1027 (Context #5B IMPs). Two sites (panels B and D) are shown in both optical image (left column)  
 1028 and with color topography map overlain (right column; red and white colors are higher  
 1029 elevations and purple and magenta colors are lower elevations); the other sites are shown in  
 1030 optical images only. (A) #6 IMP (in the Braden et al. (2014) catalog), 10.46°N, 23.547°E, LROC  
 1031 NAC M1230568264R. (B) #10 IMP, 7.559°N, 20.984°E, NAC M1144665397 and NAC DTM  
 1032 topography. (C) #28 IMP, 38.152°N, 44.6°W, NAC M1154521777L. (D) #35 IMP, 8.279°N,  
 1033 9.319°E, Kaguya TC morning map and TC DTM topography. (E) #51 IMP, 14.597°N,  
 1034 33.979°W, NAC M1142674596. (F) #60 IMP, 9.012°N, 22.248°E, TC morning map. (H) #61  
 1035 IMP, 9.738°N, 22.32°E, NAC M1096351025R. (I) #64 IMP, 14.468°N, 33.729°W, TC morning  
 1036 map. The IMPs are all marked by the white elongated triangles.



1037

1038 **Figure 12.** Geological context of Aristarchus North IMP (25.044°N, 46.767°W): (A)  
 1039 SLDEM2015 topography overlain on LROC WAC low-sun image, (B) FeO abundance map  
 1040 calculated from Kaguya Multiband Imager (MI) data using the Lemelin et al. (2015) algorithm,  
 1041 (C) LROC NAC frame M1114476549 and (D) NAC DTM topography overlain NAC  
 1042 M1114476549. The white rectangles in panels A and B mark the extent of panel C/D, the white  
 1043 polygons in panels A and B are the mare boundary mapped by Nelson et al. (2014) and the white  
 1044 arrows in panel C point to the two clusters of small IMPs.

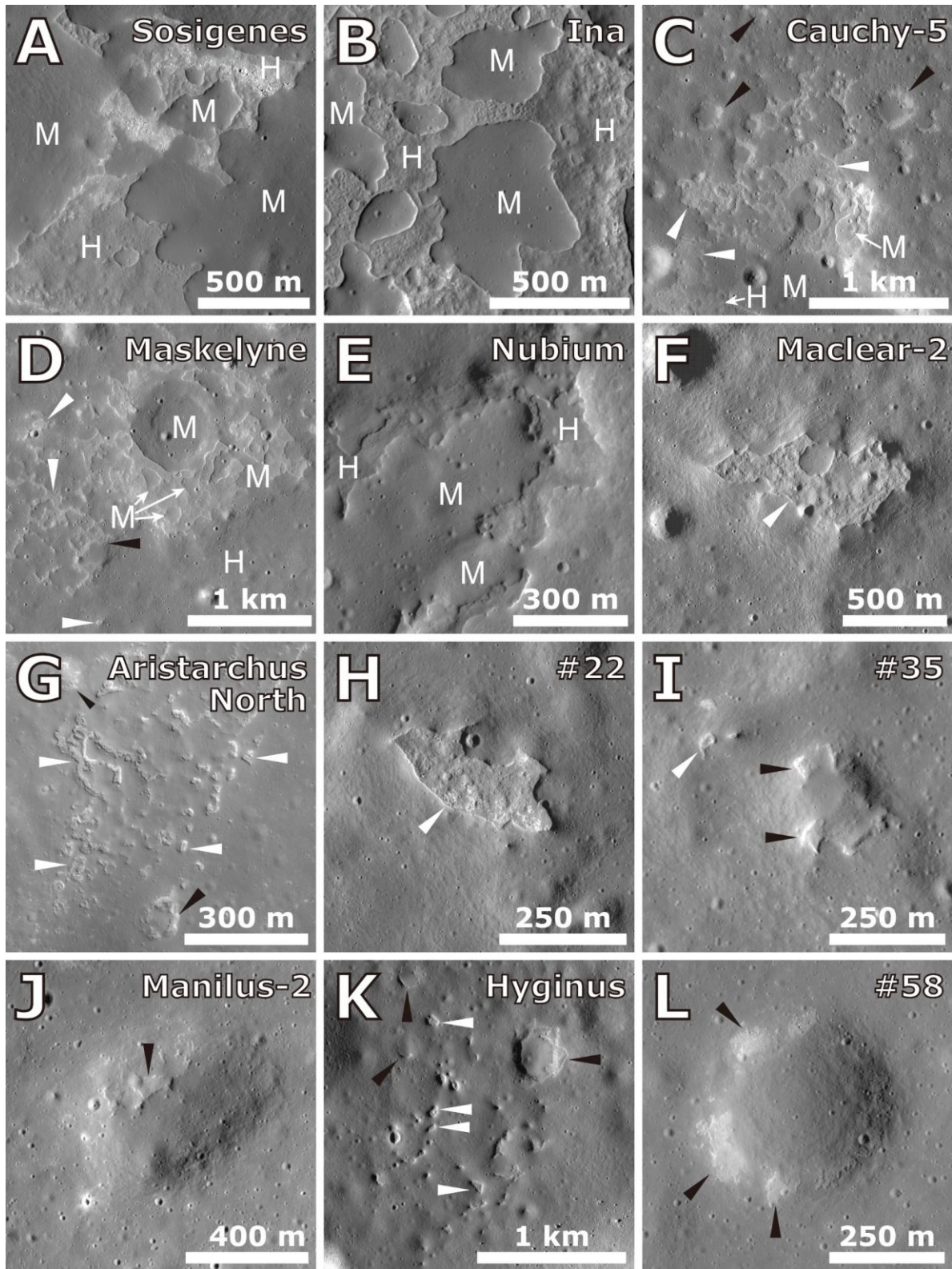


1045

1046

1047

**Figure 13.** Spatial distribution of all identified IMPs in terms of the classification of their characteristics and structure.



1048

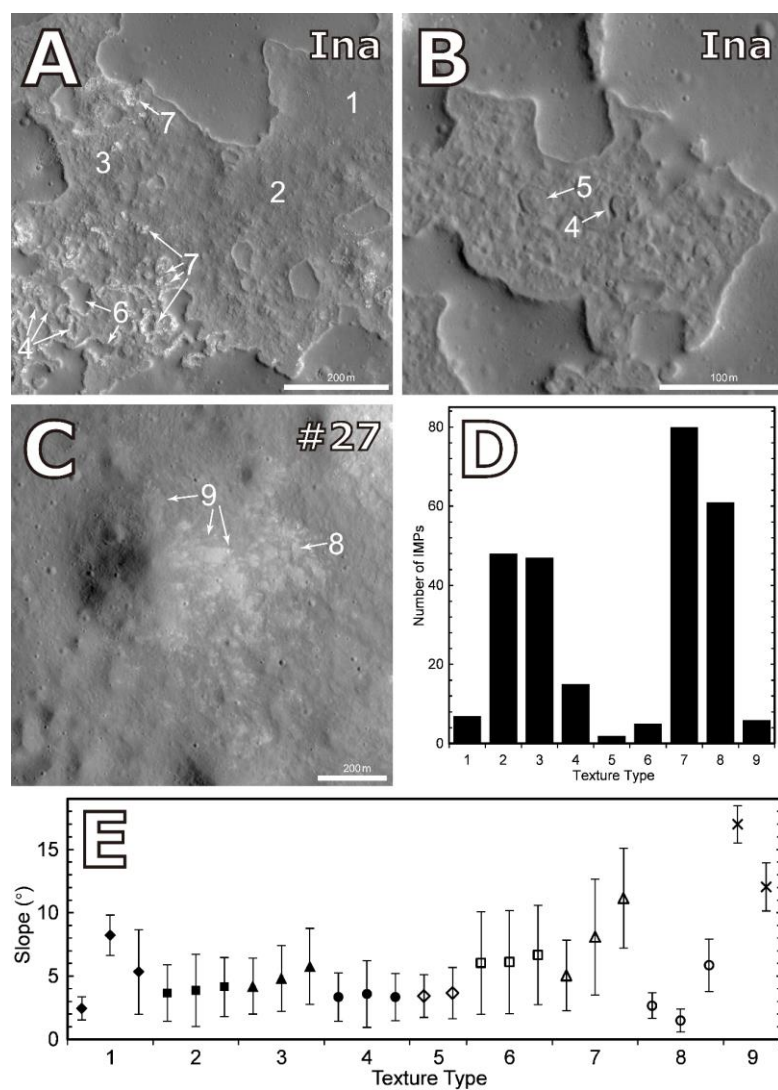
1049

1050

1051

**Figure 14.** Detailed characteristics of representative IMPs in each type: being composed of a combination of mounds and lower rough hummocky terrains (Class #1, panels A-E) and being composed of rough, bright pit terrains within mare surface (Class #2A, panels C, D, F-I and K)

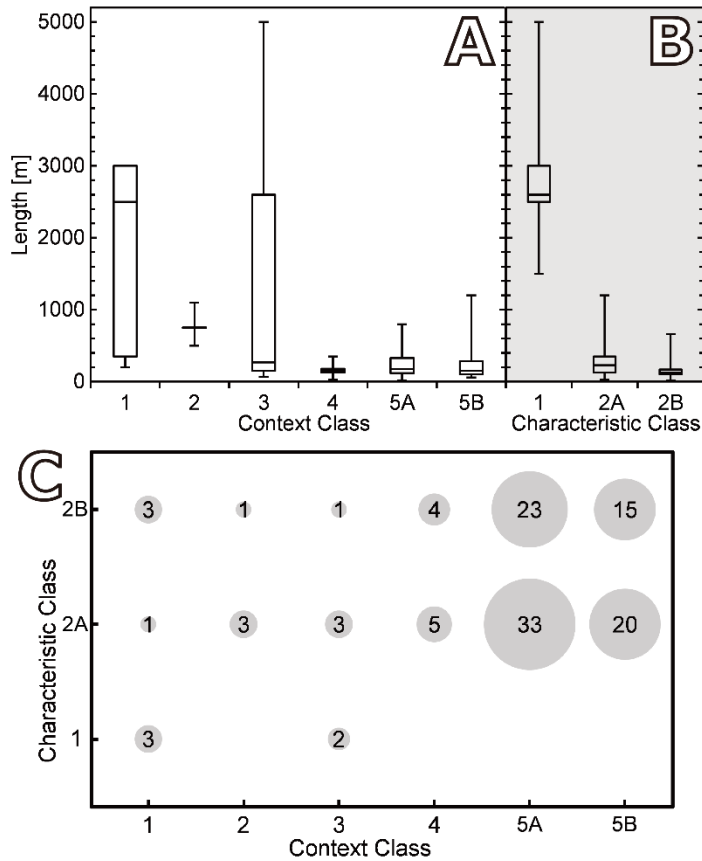
1052 and associated with depressions (Class #2B, panels C, D, G, I, J-L). (A) Sosigenes, 8.335°N,  
 1053 19.071°E, LROC NAC M192824968. (B) Ina, 18.65°N, 5.3°E, NAC M1138873574. (C)  
 1054 Cauchy-5, 7.169°N, 37.592°E, NAC M1218710334L. (D) Maskelyne, 4.33°N, 33.75°E, NAC  
 1055 M1215204344. (E) Nubium, 25.724°S, 27.681°W, NAC M1142616950L. (F) Maclear-2,  
 1056 9.102°N, 20.298°E, NAC M1276451476R. (G) Aristarchus North IMP, 25.044°N, 46.767°W,  
 1057 NAC 168509312R. (H) #22 IMP, 9.54°N, 20.22°E, NAC M162175239L. (I) #35 IMP, 8.279°N,  
 1058 9.319°E, NAC M1123533772L. (J) Manilus-2, 14.628°N, 6.821°E, NAC M192910855R. (K)  
 1059 Hyginus IMP, 7.726°N, 6.35°E, NAC M1157706629. (L) #58 IMP, 2.008°S, 43.333°E, NAC  
 1060 M1230441915R. The mounds and hummocky terrains of Class #1 IMPs are marked with “M”  
 1061 and “H”, respectively. Class #2A and #2B IMPs are marked with the white and black elongated  
 1062 triangles, respectively. The rough terrains are observed to have various surface textures and the  
 1063 most common texture types are, in descending order, blocky, uneven, hummocky and pitted floor  
 1064 textures.



1065

1066 **Figure 15.** Various types of surface textures of the floor terrains of lunar IMPs presented at (A)  
 1067 the southeastern margin of Ina floor (centered at 18.642°N, 5.331°E), LROC NAC M119815703

1068 (also for panel B), (B) the central floor of Ina (centered at 18.668°N, 5.303°E) and (C) #27 IMP,  
 1069 NAC M1173279016L. The surface texture types are marked with numbers: 1) smooth terrain, 2)  
 1070 hummocky, 3) pitted, 4) ridged, 5) polygonal, 6) vermicular, 7) blocky, 8) uneven and 9) bright  
 1071 streak. (D) The histogram of IMP population having each texture type. (E) The LROC NAC  
 1072 DTM-slope (mean value  $\pm 1\sigma$ ) of the various surface texture types at representative lunar IMPs:  
 1073 #1–7 texture types are of the Ina floor terrain, #8 texture type is of Cauchy-5 shield flank pits and  
 1074 #9 texture type is of #64 and Bessarion-V-3 IMPs.



1075

1076 **Figure 16.** The minimum, first quartile, median, third quartile and maximum length of the entire  
 1077 IMP population in each (A) context and (B) characteristic class, and (C) the occurrence  
 1078 frequency (proportional to the bubble size) of lunar IMPs in terms of their context (horizontal  
 1079 axis) and characteristic classes (vertical axis).